Title: On-demand biomanufacturing of protective conjugate vaccines

One sentence summary: *In vitro* conjugate vaccine expression technology (iVAX) enables rapid and portable biosynthesis of protective antibacterial vaccines.

Authors: Jessica C. Stark,[1,2,3,] † Thapakorn Jaroentomeechai,[4,] † Tyler D. Moeller,[4] Jasmine M. Hershewe,[1,2,3] Katherine F. Warfel,[1,2,3] Bridget S. Moricz,[5] Anthony M. Martini,[5] Rachel S. Dubner,[6] Karen J. Hsu,[7] Taylor C. Stevenson,[8] Bradley D. Jones,[5,9] Matthew P. DeLisa,[4,8,*] and Michael C. Jewett [1,2,3,10,11,*]

Affiliations:
[1]Department of Chemical and Biological Engineering, Northwestern University, 2145 Sheridan Rd Technological Institute E136, Evanston, IL USA, 60208-3120
[2]Center for Synthetic Biology, Northwestern University, 2145 Sheridan Rd Technological Institute E136, Evanston, IL USA, 60208-3120
[3]Chemistry of Life Processes Institute, Northwestern University, 2170 Campus Drive, Evanston, IL USA, 60208-3120
[4]Robert Frederick Smith School of Chemical and Biomolecular Engineering, Cornell University, 120 Olin Hall, Ithaca, NY USA, 14853
[5]Department of Microbiology and Immunology, University of Iowa, 51 Newton Rd 3-403 Bowen Science Building, Iowa City, IA 52242
[6]Department of Biological Sciences, Northwestern University, 2205 Tech Drive Hogan Hall 2144, Evanston, IL USA, 60208-3500
[7]Department of Mechanical Engineering, Northwestern University, 2145 Sheridan Rd Technological Institute B224, Evanston, IL USA, 60208-3120
[8]Nancy E. and Peter C. Meinig School of Biomedical Engineering, Cornell University, Weill Hall, Ithaca, NY USA, 14853
[9]Graduate Program in Genetics, 431 Newton Rd, University of Iowa, Iowa City, IA 52242
[10]Robert H. Lurie Comprehensive Cancer Center, Northwestern University, 676 N. St Clair St, Suite 1200, Chicago, IL, USA, 60611-3068
[11]Simpson-Querrey Institute, Northwestern University, 303 E. Superior St, Suite 11-131 Chicago, IL USA, 60611-2875

† These authors contributed equally to this work

[*]Correspondence to:

Dr. Matthew P. DeLisa
Robert Frederick Smith School of Chemical and Biomolecular Engineering
Cornell University
254 Olin Hall
Ithaca, NY 14853
Tel: +1 607-254-8560
Email: md255@cornell.edu

Dr. Michael C. Jewett
Department of Chemical and Biological Engineering
Northwestern University
2145 Sheridan Road, Technological Institute E136

Evanston, IL 60208-3120
Tel: +1 847-467-5007
E-mail: m-jewett@northwestern.edu

Abstract

Conjugate vaccines are among the most effective methods for preventing bacterial infections. However, existing manufacturing approaches limit access to conjugate vaccines due to centralized production and cold chain distribution requirements. To address these limitations, we developed a modular technology for *in vitro* conjugate vaccine expression (iVAX) in portable, freeze-dried lysates from detoxified, nonpathogenic *Escherichia coli.* Upon rehydration, iVAX reactions synthesize clinically relevant doses of conjugate vaccines against diverse bacterial pathogens in one hour. We show that iVAX-synthesized vaccines against *Francisella tularensis* subsp. *tularensis* (type A) strain Schu S4 protected mice from lethal intranasal *F. tularensis* challenge. The iVAX platform promises to accelerate development of new conjugate vaccines with increased access through refrigeration-independent distribution and portable production.

Keywords

Conjugate vaccines, cell-free protein synthesis, synthetic biology, protein engineering, on-demand biosynthesis, decentralized biomanufacturing, glycoprotein

Introduction

Drug-resistant bacteria are predicted to threaten up to 10 million lives per year by 2050 (*1*), necessitating new strategies to develop and distribute antibiotics and vaccines. Conjugate vaccines, typically composed of a pathogen-specific capsular (CPS) or O-antigen polysaccharide (O-PS) linked to an immunostimulatory protein carrier, are among the safest and most effective methods for preventing life-threatening bacterial infections (*2-4*). In particular, implementation of meningococcal and pneumococcal conjugate vaccines have significantly reduced the occurrence of bacterial meningitis and pneumonia worldwide (*5, 6*), in addition to reducing the frequency of antibiotic resistance in targeted strains (*7*). However, despite their proven safety and efficacy, global childhood vaccination rates for conjugate vaccines remain as low as ~30%, with lack of access or low immunization coverage accounting for the vast majority of remaining disease burden (*8*). In addition, the 2018 WHO prequalification of Typhbar-TCV® to prevent typhoid fever represents the first conjugate vaccine approval in nearly a decade. In order to address emerging drug-resistant pathogens, new platform technologies to accelerate the development and global distribution of conjugate vaccines are urgently needed.

Contributing to the slow pace of conjugate vaccine development and distribution is the fact that these molecules are particularly challenging and costly to manufacture. The conventional process to produce conjugate vaccines involves chemical conjugation of carrier proteins with polysaccharide antigens purified from large-scale cultures of pathogenic bacteria. Large-scale fermentation of pathogens results in high manufacturing costs due to associated biosafety hazards and process development challenges. In addition, chemical conjugation can alter the structure of the polysaccharide, resulting in loss of the protective epitope (*9*). To address these challenges, it was recently demonstrated that polysaccharide-protein conjugates can be made in *Escherichia coli* using protein-glycan coupling technology (PGCT) (*10*). In this approach, engineered *E. coli* cells covalently attach heterologously expressed CPS or O-PS antigens to

carrier proteins via an asparagine-linked glycosylation reaction catalyzed by the *Campylobacter jejuni* oligosaccharyltransferase enzyme PglB (*Cj*PglB) (*11-17*). Despite this advance, both chemical conjugation and PGCT approaches rely on living bacterial cells, requiring centralized production facilities from which vaccines are distributed via a refrigerated supply chain.

Refrigeration of conjugate vaccines is critical to avoid spoilage due to aggregate formation and significant loss of the pathogen-specific polysaccharide upon heating and freezing (*18-23*). Due to complexities and costs associated with cold chain refrigeration, vaccines with even short-term thermostability offer significant advantages. The availability of effective and thermostable freeze-dried vaccines is cited as a key technological innovation that enabled the global eradication of smallpox, the only infectious disease to be eradicated to date (*24*). Development of MenAfriVac™, a meningococcal conjugate vaccine shown to remain active outside of the cold chain for up to 4 days, enabled increased vaccine coverage and an estimated 50% reduction in costs during vaccination in the meningitis belt of sub-Saharan Africa (*25*). However, this required significant ($70M) investment in the development and validation of a thermostable vaccine. Further, conjugate vaccine thermostability varies for different O-PS antigens both across pathogens and between serotypes of the same pathogen, even in lyophilized formulations (*20-23*). Thus, generalizable strategies to achieve thermostability in the context of current manufacturing and distribution strategies may well prove elusive. Broadly, the need for cold chain refrigeration creates economic and logistical challenges that limit the reach of vaccination campaigns and present barriers to the eradication of disease, especially in low and middle income countries (*8, 26*).

Cell-free protein synthesis (CFPS) offers opportunities to both accelerate vaccine development and enable decentralized, cold chain-independent biomanufacturing by using cell lysates, rather than living cells, to synthesize proteins *in vitro* (*27*). Importantly, CFPS platforms (i) enable point-of-care protein production, as relevant amounts of protein can be synthesized *in vitro* in just a few hours, (ii) can be freeze-dried for distribution at ambient temperature and

reconstituted by just adding water (*28*), and (iii) circumvent biosafety concerns associated with the use of living cells outside of a controlled laboratory setting. CFPS has recently been used to enable on-demand and portable production of aglycosylated protein subunit vaccines (*28, 29*). However, the production of efficacious glycoprotein products, which represent 70% of approved therapeutics (*30*), from decentralized biomanufacturing platforms has not yet been demonstrated. As a result, there remains a need for additional technologies that enable decentralized production of glycosylated protein products, including conjugate vaccines.

To address this technological gap, here we describe the iVAX (*in vitro* conjugate vaccine expression) platform that enables rapid development and cold chain-independent biosynthesis of conjugate vaccines in cell-free reactions (**Figure 1**). iVAX was designed to have the following features. First, iVAX is fast, with the ability to produce multiple individual doses of conjugates in one hour. Second, iVAX is robust, yielding equivalent amounts of conjugate over a range of operating temperatures. Third, iVAX is modular, offering the ability to rapidly interchange carrier proteins, including those used in licensed conjugate vaccines, as well as conjugated polysaccharide antigens. We leverage this modularity to create an array of vaccine candidates targeted against diverse bacterial pathogens, including the highly virulent *Francisella tularensis* subsp. *tularensis* (type A) strain Schu S4, enterotoxigenic (ETEC) *E. coli* O78, and uropathogenic (UPEC) *E. coli* O7. Fourth, iVAX is shelf-stable, derived from freeze-dried cell-free reactions that operate in a just-add-water strategy. Fifth, iVAX is safe, leveraging lipid A engineering that effectively avoids the high levels of endotoxin present in wild-type *E. coli*. Our results demonstrate that a *F. tularensis* O-PS conjugate derived from freeze-dried, low-endotoxin iVAX reactions outperformed a conjugate produced using the established cell-based PGCT approach in its ability to elicit pathogen-specific antibodies. Moreover, the iVAX-derived conjugate afforded complete protection in a mouse model of intranasal *F. tularensis* infection. Overall, the iVAX platform offers a new way to deliver the protective benefits of an important class of antibacterial vaccines to both the developed and developing world.

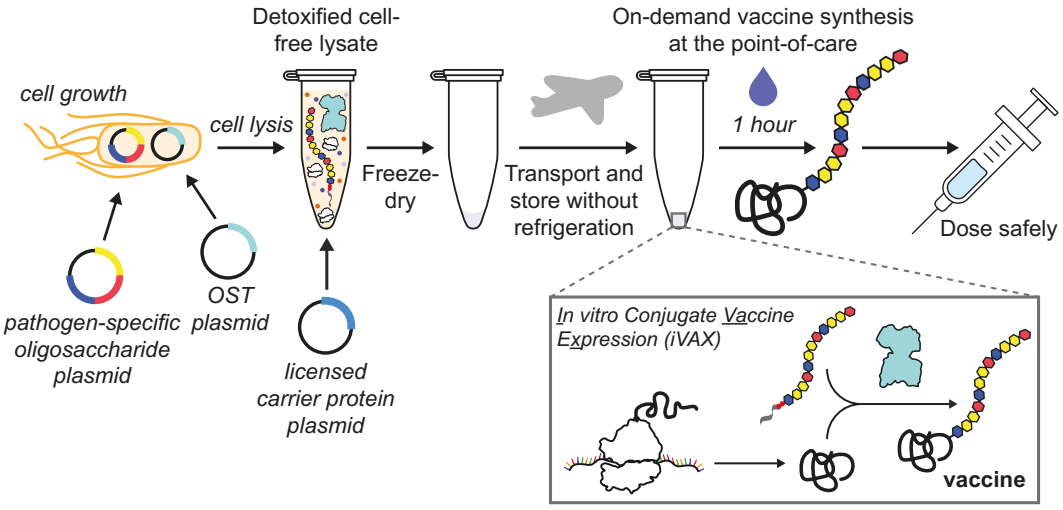

Figure 1. iVAX platform enables on-demand and portable production of antibacterial vaccines. The *in vitro* conjugate vaccine expression (iVAX) platform provides a rapid means to develop and distribute conjugate vaccines against bacterial pathogens. Expression of pathogen-specific polysaccharide antigens (e.g., CPS, O-PS) and a bacterial oligosaccharyltransferase enzyme in nonpathogenic *E. coli* with detoxified lipid A yields low-endotoxin lysates containing all of the machinery required for synthesis of conjugate vaccines. Reactions catalyzed by iVAX lysates can be used to produce conjugates containing licensed carrier proteins and can be freeze-dried without loss of activity for refrigeration-free transportation and storage. Freeze-dried reactions can be activated at the point-of-care via simple rehydration and used to reproducibly synthesize immunologically active conjugate vaccines in ~1 h.

Results

***In vitro* synthesis of licensed vaccine carrier proteins.** To demonstrate proof-of-principle for cell-free conjugate vaccine production, we first set out to express a set of carrier proteins that are currently used in approved conjugate vaccines. Producing these carrier proteins in soluble conformations *in vitro* represented an important benchmark because their expression in living *E. coli* has proven challenging, often requiring multi-step purification and refolding of insoluble product from inclusion bodies (*31, 32*), fusion of expression partners such as maltose-binding protein (MBP) to increase soluble expression (*32, 33*), or expression of truncated protein variants in favor of the full-length proteins (*33*). In contrast, cell-free protein synthesis approaches have recently shown promise for difficult-to-express proteins (*34*). The carrier proteins that we focused

on here included nonacylated *H. influenzae* protein D (PD), the *N. meningitidis* porin protein (PorA), and genetically detoxified variants of the *Corynebacterium diphtheriae* toxin (CRM197) and the *Clostridium tetani* toxin (TT). We also tested expression of the fragment C (TTc) and light chain (TTlight) domains of TT as well as *E. coli* MBP. While MBP is not a licensed carrier, it has demonstrated immunostimulatory properties (*35*) and when linked to O-PS was found to elicit polysaccharide-specific humoral and cellular immune responses in mice (*13*). Similarly, the TT domains, TTlight and TTc, have not been used in approved vaccines, but are immunostimulatory and individually sufficient for protection against *C. tetani* challenge in mice (*33*). To enable conjugation with O-PS antigens, all carriers were modified at their C-termini with 4 tandem repeats of an optimal bacterial glycosylation motif, DQNAT (*36*). A C-terminal 6xHis tag was also included to enable purification and detection via Western blot analysis. A variant of superfolder green fluorescent protein that contained an internal DQNAT glycosylation site (sfGFP$^{217\text{-}DQNAT}$) (*37*) was used as a model protein to facilitate system development.

All eight carriers were synthesized *in vitro* with soluble yields of ~50-650 μg mL^{-1} as determined by ^{14}C-leucine incorporation (**Figure 2a**). In particular, the MBP^{4xDQNAT} and PD^{4xDQNAT} variants were nearly 100% soluble, with yields of 500 μg mL^{-1} and 200 μg mL^{-1}, respectively, and expressed as exclusively full-length products according to Western blot and autoradiogram analysis (**Figure 2c, figure S1a**). Notably, similar soluble yields were observed for all carriers at 25°C, 30°C, and 37°C, with the exception of CRM197^{4xDQNAT} (**figure S1b**), which is known to be heat sensitive (*19*). These results suggest that our method of cell-free carrier biosynthesis is robust over a 13°C range in temperature and could be used in settings where precise temperature control is not feasible.

The open reaction environment of our cell-free reactions enabled facile manipulation of the chemical and reaction environment to improve production of more complex carriers. For example, in the case of the membrane protein PorA^{4xDQNAT}, lipid nanodiscs were added to increase soluble expression (**figure S1c**). Nanodiscs provide a cellular membrane mimic to co-

translationally stabilize hydrophobic regions of membrane proteins (*38*). For expression of TT, which contains an intermolecular disulfide bond, expression was carried out for 2 hours in oxidizing conditions (*39*), which improved assembly of the heavy and light chains into full-length product and minimized protease degradation of full-length TT (**figure S1d**). While full-length protein production could be further optimized in the future, this represents the first example of recombinant expression of full-length TT, to our knowledge. Western blot analysis of *in vitro* synthesized $CRM197^{4xDQNAT}$ and $TT^{4xDQNAT}$ revealed species that were comparable in size to commercially available purified diphtheria toxin (DT) and TT protein standards (**figure S1e**). Lower molecular weight species were also observed, which we hypothesize result from protease degradation of full length $CRM197^{4xDQNAT}$ and $TT^{4xDQNAT}$ following translation. These species could be mitigated by incorporating a size-based separation step into decentralized production (*29*), as previously described. In addition, full length $CRM197^{4xDQNAT}$ and $TT^{4xDQNAT}$ were reactive with αDT and αTT antibodies, respectively (**figure S1f**), indicating that immunogenic epitopes were faithfully synthesized. This is notable as CRM197 and TT are FDA-approved vaccine antigens for diphtheria and tetanus, respectively, when they are administered without conjugated polysaccharides. Together, our results highlight the ability of CFPS to express licensed conjugate vaccine carrier proteins in soluble conformations over a range of temperatures.

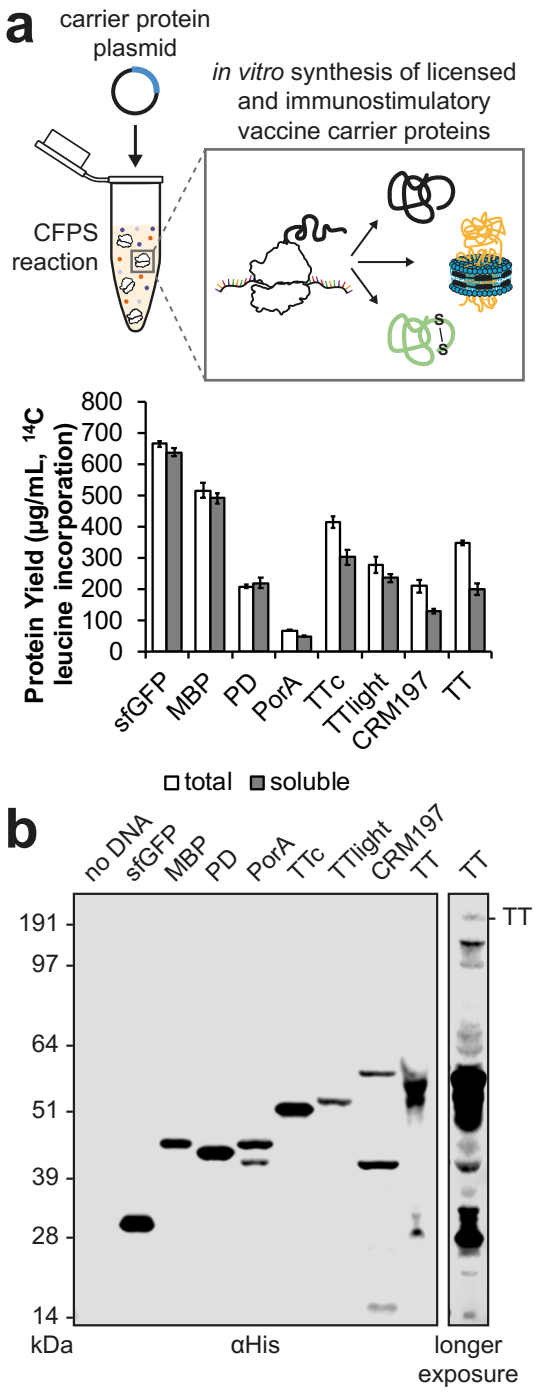

Figure 2. *In vitro* synthesis of licensed conjugate vaccine carrier proteins. (**a**) All four carrier proteins used in approved conjugate vaccines were synthesized solubly *in vitro*, as measured via ^{14}C-leucine incorporation. These include *H. influenzae* protein D (PD), the *N. meningitidis* porin protein (PorA), and genetically detoxified variants of the *C. diphtheriae* toxin (CRM197) and the *C. tetani* toxin (TT). Additional immunostimulatory carriers, including *E. coli* maltose binding protein (MBP) and the fragment C (TTc) and light chain (TTlight) domains of TT, were also synthesized solubly. Values represent means and error bars represent standard deviations of biological replicates (n = 3). (**b**) Full length product was observed for all proteins tested via

Western blot. Different exposures are indicated with solid lines. Molecular weight ladder is shown at left.

On-demand biosynthesis of conjugate vaccines. We next sought to synthesize polysaccharide-conjugated versions of these carrier proteins by co-activating their *in vitro* expression with cell-free glycosylation in a one-pot reaction. As a model vaccine target, we focused on the highly virulent *F. tularensis* subsp. *tularensis* (type A) strain Schu S4, a gram-negative, facultative coccobacillus and the causative agent of tularemia. This bacterium is categorized as a class A bioterrorism agent due to its high fatality rate, low dose of infection, and ability to be aerosolized (*40, 41*). Vaccines targeting *F. tularensis* will likely need to be deployed rapidly using ring vaccination strategies in response to an outbreak, similar to those planned in the event of a smallpox attack (*42*) and used to eradicate smallpox in the 1960s and 70s (*24*). We thus sought to develop rapidly deployable, thermostable conjugate vaccines against *F. tularensis* as an initial demonstration of the iVAX technology.

Although there are currently no approved vaccines against *F. tularensis*, several studies have independently confirmed the important role of antibodies directed against *F. tularensis* LPS, specifically the O-PS repeat unit, in providing protection against the Schu S4 strain (*43, 44*). More recently, a conjugate vaccine comprising the *F. tularensis* Schu S4 O-PS (*Ft*O-PS) conjugated to the *Pseudomonas aeruginosa* exotoxin A ($EPA^{DNNNS\text{-}DQNRT}$) carrier protein produced using PGCT (*14, 15*) was shown to be protective against challenge with the Schu S4 strain in a rat inhalation model of tularemia (*15*). In light of these earlier findings, we investigated the ability of the iVAX platform to produce anti-*F. tularensis* conjugate vaccine candidates on-demand by conjugating the *Ft*O-PS structure to diverse carrier proteins *in vitro*.

The *Ft*O-PS is composed of the 826-Da repeating tetrasaccharide unit Qui4NFm-$(GalNAcAN)_2$-QuiNAc (Qui4NFm: 4,6-dideoxy-4-formamido-D-glucose; GalNAcAN: 2-acetamido-2-deoxy-D-galacturonamide; QuiNAc: 2-acetamido-2,6-dideoxy-D-glucose) (*45*). We and other groups have previously shown that the authentic *Ft*O-PS structure can be synthesized in K-12

strains of *E. coli* via recombinant expression of the *Ft*O-PS biosynthetic pathway (*14, 45, 46*). To glycosylate proteins with *Ft*O-PS, we produced an iVAX lysate from *E. coli* cells expressing the *Ft*O-PS biosynthetic pathway and the oligosaccharyltransferase enzyme *Cj*PglB (**Figure 3a**). This lysate, which contained lipid-linked *Ft*O-PS and active *Cj*PglB, was used to catalyze iVAX reactions primed with plasmid DNA encoding sfGFP$^{217\text{-}DQNAT}$. Control reactions in which attachment of the *Ft*O-PS was not expected were performed with lysates from cells that lacked either the *Ft*O-PS pathway or the *Cj*PglB enzyme. We also tested reactions that lacked plasmid encoding the target protein sfGFP$^{217\text{-}DQNAT}$ or were primed with plasmid encoding sfGFP$^{217\text{-}AQNAT}$, which contained a mutated glycosylation site (AQNAT) that is not modified by *Cj*PglB (*47*). In reactions containing the iVAX lysate and primed with plasmid encoding sfGFP$^{217\text{-}DQNAT}$, immunoblotting with anti-His antibody or a commercial monoclonal antibody specific to *Ft*O-PS revealed a ladder-like banding pattern (**Figure 3b**). This ladder is characteristic of *Ft*O-PS attachment, resulting from O-PS chain length variability through the action of the Wzy polymerase (*10, 14, 45*). Glycosylation of sfGFP$^{217\text{-}DQNAT}$ was observed only in reactions containing a complete glycosylation pathway and the preferred DQNAT glycosylation sequence (**Figure 3b**). This glycosylation profile was further reproducible across biological replicates from the same lot of lysate (**Figure 3c, left**) and using different lots of lysate (**Figure 3c, right**), with an average efficiency of conjugation with *Ft*O-PS of 69 ± 5% by densitometry analysis. *In vitro* protein synthesis and glycosylation was observed after 1 hour, with the amount of conjugated polysaccharide reaching a maximum between 45 and 75 minutes (**figure S2**). Similar glycosylation reaction kinetics were observed at 37°C, 30°C, 25°C, and room temperature (~21°C), indicating that iVAX reactions are robust over a range of temperatures (**figure S2**).

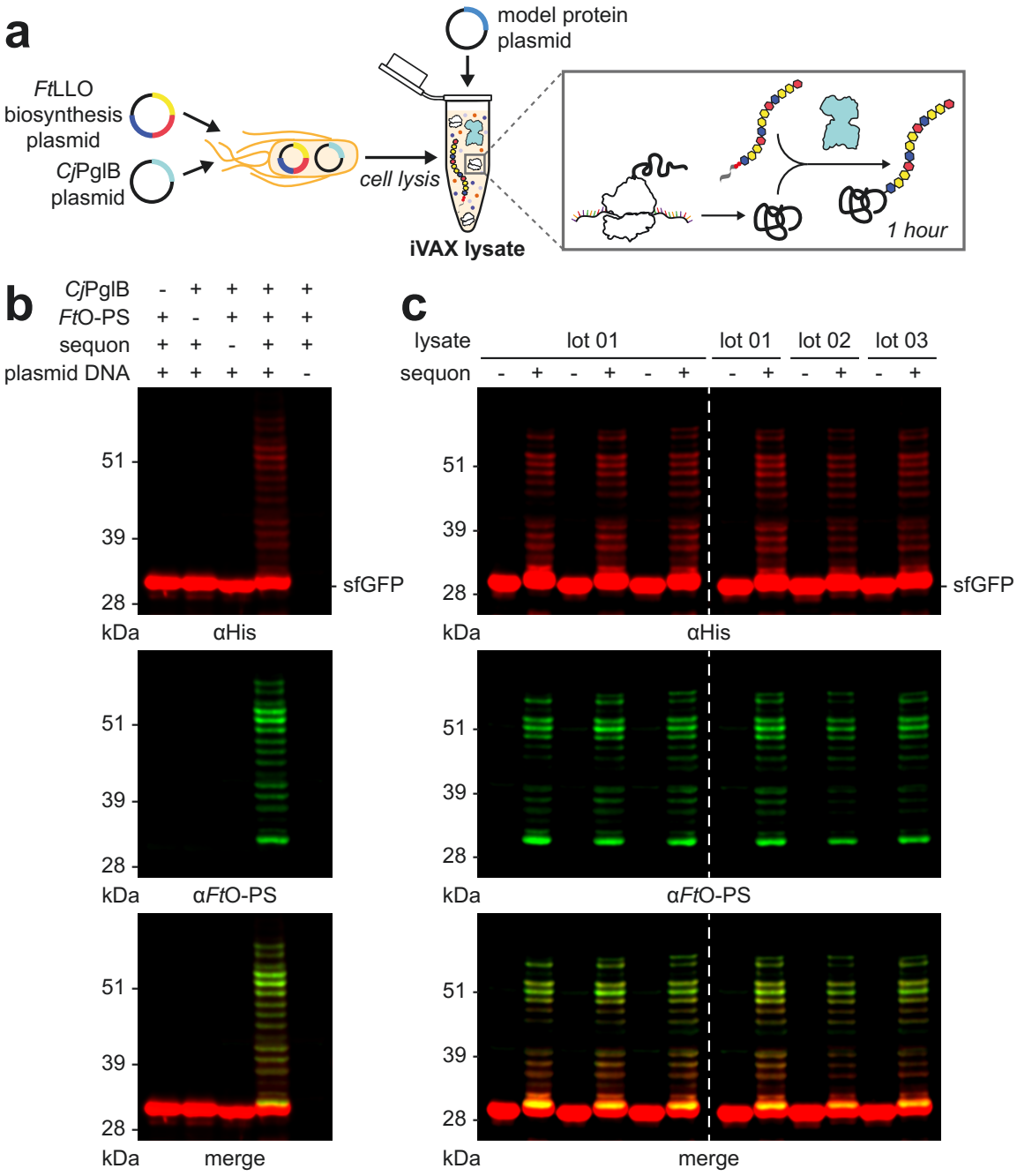

Figure 3. Reproducible glycosylation of proteins with *Ft*O-PS in iVAX. (**a**) iVAX lysates were prepared from cells expressing *Cj*PglB and a biosynthetic pathway encoding *Ft*O-PS. (**b**) Glycosylation of sfGFP$^{217\text{-}DQNAT}$ with *Ft*O-PS was only observed when *Cj*PglB, *Ft*O-PS, and the preferred glycosylation sequence (sequon) were present in the reaction (lane 3). When plasmid DNA was omitted, sfGFP$^{217\text{-}DQNAT}$ synthesis was not observed. (**c**) Biological replicates of iVAX reactions producing sfGFP$^{217\text{-}DQNAT}$ using the same lot (**left**) or different lots (**right**) of iVAX lysates demonstrated reproducibility of reactions and lysate preparation. Top panels show signal from probing with anti-hexa-histidine antibody (αHis) to detect the carrier protein, middle panels show signal from probing with commercial anti-*Ft*O-PS antibody (α*Ft*O-PS), and bottom panels show αHis and α*Ft*O-PS signals merged. Images are representative of at least three biological

replicates. Dashed lines indicate samples are from nonadjacent lanes of the same blot with the same exposure. Molecular weight ladders are shown at the left of each image.

Next, we investigated whether immunologically relevant carriers could be similarly conjugated with *Ft*O-PS in iVAX reactions. Following addition of plasmid DNA encoding MBP^{4xDQNAT}, PD^{4xDQNAT}, PorA^{4xDQNAT}, TTc^{4xDQNAT}, TTlight^{4xDQNAT}, CRM197^{4xDQNAT}, or the most common PGCT carrier protein, EPA$^{DNNNS-DQNRT}$ (*12, 14-17*), glycosylation of each with *Ft*O-PS was observed for iVAX reactions enriched with lipid-linked *Ft*O-PS and *Cj*PglB but not control reactions lacking *Cj*PglB (**Figure 4**). Notably, our attempts to synthesize the same panel of conjugates using the established PGCT approach in living *E. coli* yielded less promising results. Specifically, only limited expression of conjugates composed of PorA and CRM197, two of the carriers used in licensed conjugate vaccines, were achieved *in vivo* (**figure S3**). Collectively, these data indicate that iVAX may provide advantages over the established PGCT approach for production of conjugate vaccine candidates composed of diverse and potentially membrane-bound carrier proteins.

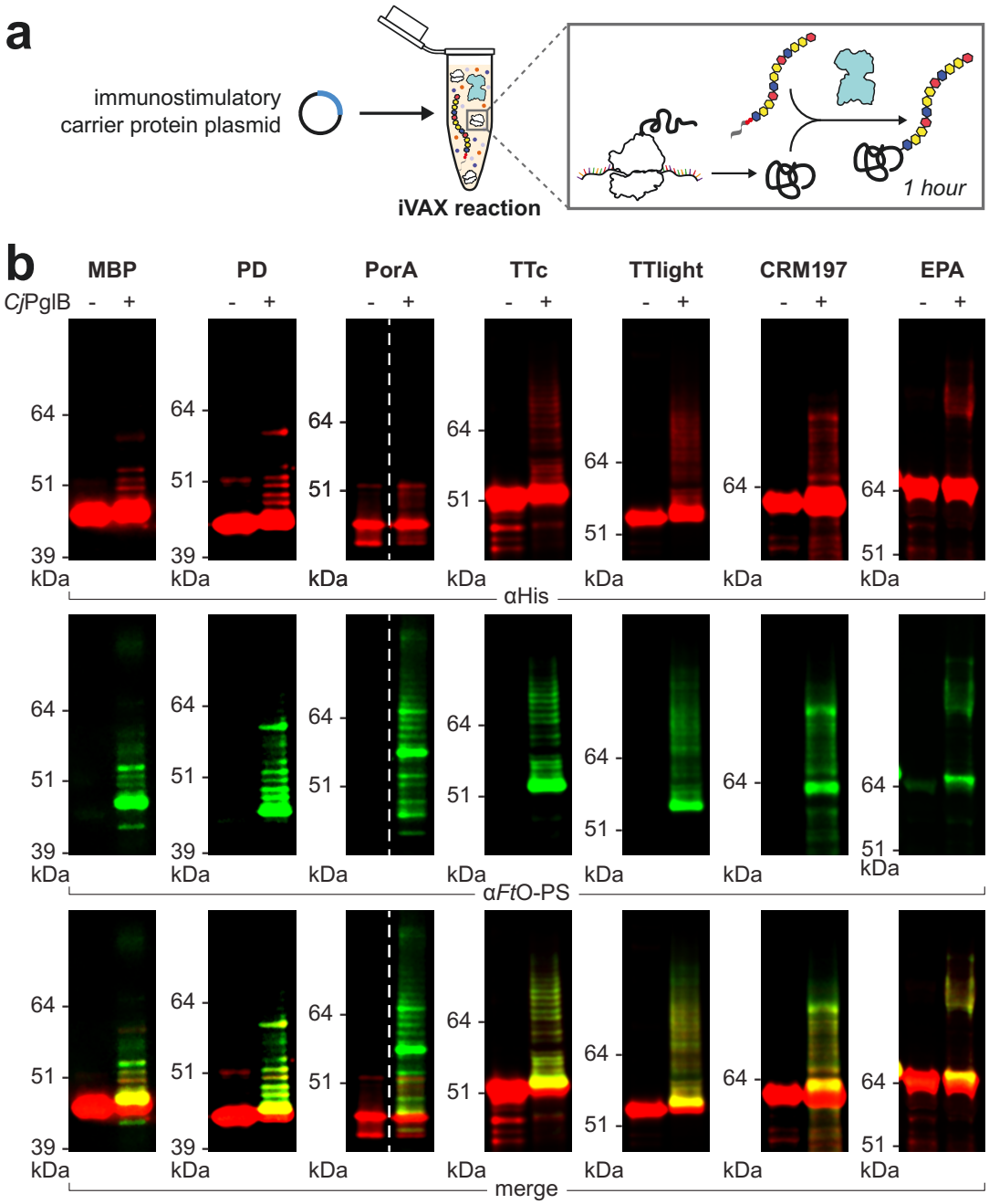

Figure 4. On-demand production of conjugate vaccines against *F. tularensis* using iVAX. (**a**) iVAX reactions were prepared from lysates containing *Cj*PglB and *Ft*O-PS and primed with plasmid encoding immunostimulatory carriers, including those used in licensed vaccines. (**b**) We observed on-demand synthesis of anti-*F. tularensis* conjugate vaccines for all carrier proteins tested. Conjugates were purified using Ni-NTA agarose from 1 mL iVAX reactions lasting ~1 h. Top panels show signal from probing with anti-hexa-histidine antibody (αHis) to detect the carrier protein, middle panels show signal from probing with commercial anti-*Ft*O-PS antibody (α*Ft*O-PS), and bottom panels show αHis and α*Ft*O-PS signals merged. Images are representative of at least three biological replicates. Dashed lines indicate samples are from

nonadjacent lanes of the same blot with the same exposure. Molecular weight ladders are shown at the left of each image.

We next asked whether the yields of conjugates produced using iVAX were sufficient to enable production of relevant vaccine doses. To assess expression titers, we focused on $MBP^{4xDQNAT}$ and $PD^{4xDQNAT}$ because these carriers expressed *in vitro* with high soluble titers and as exclusively full-length protein (**Figure 2, figure S1a**). In addition, PD has been shown to be a safe and effective conjugate vaccine carrier protein (*48, 49*) and may have advantages over DT and TT in generating robust immune responses to polysaccharide antigens (*50-53*). Recent clinical data show 1-10 μg doses of conjugate vaccine candidates are well-tolerated and effective in stimulating the production of antibacterial IgGs (*54-56*). We found that reactions lasting ~1 hour produced ~20 μg mL^{-1}, or two 10-μg doses mL^{-1}, of *Ft*O-PS-conjugated $MBP^{4xDQNAT}$ and $PD^{4xDQNAT}$ as determined by ^{14}C-leucine incorporation and densitometry analysis (**figure S4a**). It should be noted that vaccines are currently distributed in vials containing 1-20 doses of vaccine to minimize wastage (*57*). Our yields indicate that multiple doses per mL can be synthesized in 1 hour using the iVAX platform.

To demonstrate the modularity of the iVAX approach for conjugate vaccine production, we sought to produce conjugates bearing O-PS antigens from additional pathogens including ETEC *E. coli* strain O78 and UPEC *E. coli* strain O7. *E. coli* O78 is a major cause of diarrheal disease in low and middle income countries, especially among children, and a leading cause of traveler's diarrhea (*58*), while the O7 strain is a common cause of urinary tract infections (*59*). Like the *Ft*O-PS, the biosynthetic pathways for *Ec*O78-PS and *Ec*O7-PS have been described previously and confirmed to produce O-PS antigens with the repeating units $GlcNAc_2Man_2$ (*60*) and Qui4NAcMan(Rha)GalGlcNAc (*61*), respectively (GlcNAc: *N*-acetylglucosamine; Man: mannose; Qui4NAc: 4-acetamido-4,6-dideoxy-D-glucopyranose; Rha: rhamnose; Gal: galactose). Using iVAX lysates from cells expressing *Cj*PglB and either the *Ec*O78-PS and *Ec*O7-PS pathways in reactions that were primed with $PD^{4xDQNAT}$ or $sfGFP^{217\text{-}DQNAT}$ plasmids, we observed O-PS

conjugation only when both lipid-linked O-PS and *Cj*PglB were present in the reactions (**figure S4b, c**). These results demonstrate modular production of conjugate vaccines against multiple bacterial pathogens using iVAX, enabled by compatibility of multiple heterologous O-PS pathways with *in vitro* carrier protein synthesis and glycosylation.

Endotoxin editing and freeze-drying yield iVAX reactions that are safe and portable. A key challenge inherent in using any *E. coli*-based system for biopharmaceutical production is the presence of lipid A, or endotoxin, which is known to contaminate protein products and can cause lethal septic shock at high levels (*62*). As a result, the amount of endotoxin in formulated biopharmaceuticals is regulated by the US FDA, as well as the European Medicines Agency (*63*). Because iVAX reactions rely on lipid-associated components, such as *Cj*PglB and *Ft*O-PS, standard detoxification approaches involving the removal of lipid A (*64*) could compromise the activity or concentration of our glycosylation components, in addition to increasing cost and processing complexities.

To address this issue, we adapted a previously reported strategy to detoxify the lipid A molecule through strain engineering (*46, 65*). In particular, the deletion of the acyltransferase gene *lpxM* and the overexpression of the *F. tularensis* phosphatase LpxE in *E. coli* has been shown to result in the production of nearly homogenous pentaacylated, monophosphorylated lipid A with significantly reduced toxicity but retained adjuvanticity (*46*). This pentaacylated, monophosphorylated lipid A is structurally identical to the primary component of monophosphoryl lipid A (MPL) from *Salmonella minnesota* R595, an approved adjuvant composed of a mixture of monophosphorylated lipids (*66*). To generate detoxified lipid A structures in the context of iVAX, we produced lysates from a Δ*lpxM* derivative of CLM24 that co-expressed *Ft*LpxE and the *Ft*O-PS glycosylation pathway (**Figure 5a**). The growth rate of CLM24 Δ*lpxM* was indistinguishable from the wild-type strain, facilitating scale-up of fermentations for production of reduced-endotoxin lysates (**Figure 5b**). Lysates derived from this strain exhibited significantly decreased levels of

toxicity compared to wild type CLM24 lysates expressing *Cj*PglB and *Ft*O-PS (**Figure 5c**) as measured by human TLR4 activation in HEK-Blue hTLR4 reporter cells (*65*). Importantly, the structural remodeling of lipid A did not affect the activity of the membrane-bound *Cj*PglB and *Ft*O-PS components in iVAX reactions (**figure S5a**). By engineering the chassis strain for lysate production, we produced iVAX lysates with <1000 EU mL^{-1}. This represents a 12.5-fold average reduction in endotoxin content compared to the wild-type lysate, which we suspected would ensure acceptable endotoxin levels in purified conjugate vaccines without the need for additional removal steps. Indeed, *Ft*O-PS conjugates synthesized and affinity purified from detoxified iVAX lysates contained 0.21 ± 0.3 EU per 10-µg dose, which is well below endotoxin levels reported in commercial conjugate vaccines (<12 EU/dose) (*63, 67*) (**Figure 5d**).

A major limitation of traditional conjugate vaccines is that they must be refrigerated (*19*), making it difficult to distribute these vaccines to remote or resource-limited settings. The ability to freeze-dry iVAX reactions for ambient temperature storage and distribution could alleviate the logistical challenges associated with refrigerated supply chains that are required for existing vaccines. To investigate this possibility, detoxified iVAX lysates were used to produce *Ft*O-PS conjugates in two different ways: either by running the reaction immediately after priming with plasmid encoding the $sfGFP^{217\text{-}DQNAT}$ target protein or by running after the same reaction mixture was lyophilized and rehydrated (**Figure 5e**). In both cases, conjugation of *Ft*O-PS to $sfGFP^{217\text{-}DQNAT}$ was observed when *Cj*PglB was present, with modification levels that were nearly identical (average glycosylation efficiency of $sfGFP^{217\text{-}DQNAT}$ in reactions with and without lyophilization were 66 ± 7% and 69 ± 5% by densitometry, respectively) (**Figures 3c, 5f, and S6**). We also showed that detoxified, freeze-dried iVAX reactions can be scaled to 5 mL for production of *Ft*O-PS-conjugated $MBP^{4xDQNAT}$ and $PD^{4xDQNAT}$ in a manner that was reproducible from lot to lot and indistinguishable from production without freeze-drying (average glycosylation efficiencies of $MBP^{4xDQNAT}$ and $PD^{4xDQNAT}$ were 66 ± 10% and 70 ± 1% by densitometry, respectively) (**figure S5b, c**). In addition, freeze-dried reactions are stable under ambient temperature storage for at

least 3 months, with no observable differences in protein synthesis or glycosylation activity (**figure S6**). The ability to lyophilize iVAX reactions, store reactions at ambient temperature, and manufacture conjugate vaccines scalably and without specialized equipment highlights the potential for portable, on-demand vaccine production.

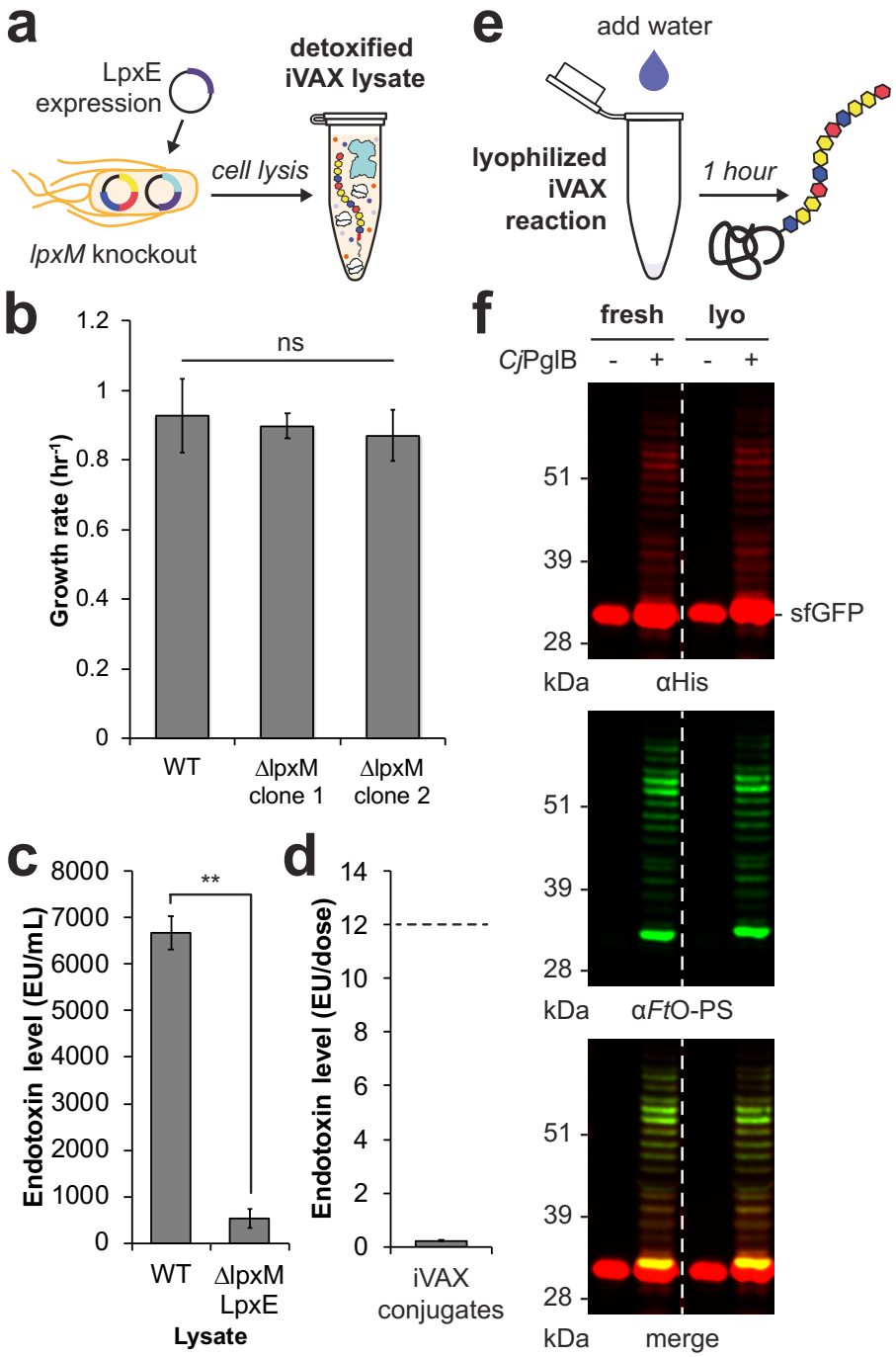

Figure 5. Detoxified, lyophilized iVAX reactions produce conjugate vaccines. (**a**) iVAX lysates were detoxified via deletion of *lpxM* and expression of *F. tularensis* LpxE in the source strain for lysate production. (**b**) Growth rates of CLM24 WT and CLM24 Δ*lpxM* strains. No growth defects were observed across two clones of the knockout strain. Values represent means and error bars represent standard deviations of $n = 4$ replicates. (**c**) The resulting lysates exhibited significantly reduced endotoxin activity, as measured by activation of human TLR4 in HEK-Blue hTLR4 reporter cells. $^{**}p = 0.003$, as determined by two-tailed *t*-test. Values represent means and error bars represent standard deviations of $n = 3$ replicates. (**d**) *Ft*O-PS conjugate vaccines produced and purified from detoxified iVAX reactions contained 0.21 ± 0.3 EU/10 μg dose, as measured by human TLR4 activation. Dashed line represents endotoxin levels reported in commercial conjugate vaccines (<12 EU/dose). Value represents mean and error bars represent standard deviation of $n = 6$ replicates. (**e**) iVAX reactions producing sfGFP$^{217\text{-}DQNAT}$ were run immediately or following lyophilization and rehydration. (**f**) Glycosylation activity was preserved following lyophilization, demonstrating the potential of iVAX reactions for portable biosynthesis of conjugate vaccines. Top panel shows signal from probing with anti-hexa-histidine antibody (αHis) to detect the carrier protein, middle panel shows signal from probing with commercial anti-*Ft*O-PS antibody (α*Ft*O-PS), and bottom panel shows αHis and α*Ft*O-PS signals merged. Images are representative of at least three biological replicates. Molecular weight ladder is shown at the left of each image.

***In vitro* synthesized conjugates elicit pathogen-specific antibodies in mice.** We next evaluated the ability of iVAX-derived conjugates to elicit anti-*Ft*LPS antibodies in mice (**Figure 6a**). Importantly, we found that BALB/c mice receiving iVAX-derived *Ft*O-PS-conjugated MBP^{4xDQNAT} or PD^{4xDQNAT} produced high titers of *Ft*LPS-specific IgG antibodies, which were significantly elevated compared to the titers measured in the sera of control mice receiving PBS or unmodified versions of each carrier protein (**Figure 6b, figure S7**). Interestingly, the IgG titers measured in sera from mice receiving PGCT-derived MBP^{4xDQNAT} conjugates were similar to the titers observed in the control groups (**Figure 6b, figure S7**). Notably, both MBP^{4xDQNAT} and PD^{4xDQNAT} conjugates produced using iVAX elicited similar levels of IgG production and neither resulted in any observable adverse events in mice, confirming the modularity and safety of the technology for production of conjugate vaccine candidates.

We further characterized IgG titers by analysis of IgG1 and IgG2a subtypes and found that both iVAX-derived *Ft*O-PS-conjugated MBP^{4xDQNAT} and PD^{4xDQNAT} boosted production of IgG1 antibodies by >2 orders of magnitude relative to all control groups as well as to PGCT-derived MBP^{4xDQNAT} conjugates (**Figure 6c**). Observed IgG subclass titers elicited by iVAX-derived

conjugates (IgG1 >> IgG2a) are further consistent with a Th2-biased response, which is characteristic of most conjugate vaccines (*68*), though additional studies are needed to confirm this immunological phenotype. Taken together, these results provide evidence that the iVAX platform supplies vaccine candidates that are capable of eliciting strong, pathogen- and polysaccharide-specific humoral immune responses.

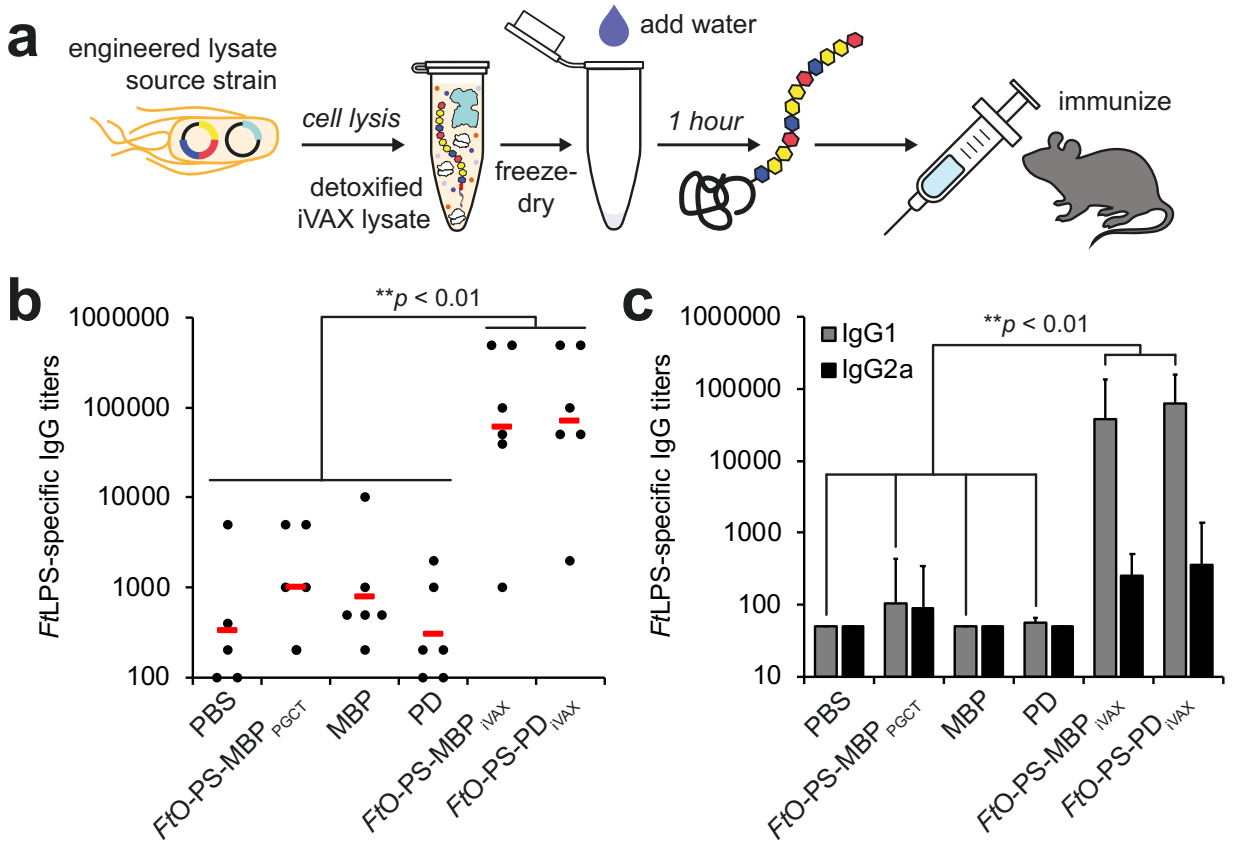

Figure 6. iVAX-derived conjugates elicit *Ft*LPS-specific antibodies and protect mice from lethal pathogen challenge. (**a**) Freeze-dried iVAX reactions assembled using detoxified lysates were used to synthesize anti-*F. tularensis* conjugate vaccines for immunization studies. (**b**) Groups of BALB/c mice were immunized subcutaneously with PBS or 7.5 µg of purified, cell-free synthesized unmodified or *Ft*O-PS-conjugated carrier proteins. *Ft*O-PS-conjugated MBP^{4xDQNAT} prepared in living *E. coli* cells using PCGT was used as a positive control. Each group was composed of six mice except for the PBS control group, which was composed of five mice. Mice were boosted on days 21 and 42 with identical doses of antigen. *Ft*LPS-specific IgG titers were measured by ELISA in endpoint (day 70) serum of individual mice (black dots) with *F. tularensis* LPS immobilized as antigen. Mean titers of each group are also shown (red lines). iVAX-derived conjugates elicited significantly higher levels of *Ft*LPS-specific IgG compared to all other groups (**$p < 0.01$, Tukey-Kramer HSD). (**c**) IgG1 and IgG2a subtype titers measured by ELISA from endpoint serum revealed that iVAX-derived conjugates boosted production of *Ft*O-PS-specific IgG1 compared to all other groups tested (**$p < 0.01$, Tukey-Kramer HSD). These results indicate

that iVAX conjugates elicited a Th2-biased immune response typical of most conjugate vaccines. Values represent means and error bars represent standard errors of *Ft*LPS-specific IgGs detected by ELISA.

iVAX-derived vaccines protect mice from lethal intranasal *F. tularensis* challenge. Finally, we tested the ability of iVAX-derived vaccines to protect mice in an intranasal model of *F. tularensis* infection (**Figure 7a**). *F. tularensis* subsp. *tularensis* SchuS4 requires biosafety level 3 containment, presenting logistical challenges for a pathogen challenge study. Instead, as a first step in assessing vaccine efficacy, we used the less virulent, but still lethal, *F. tularensis subsp. holarctica* live vaccine strain (LVS) Rocky Mountain Laboratories, which is commonly used as a *F. tularensis* challenge model (*46, 69*). We used an intranasal infection model because it represents the most challenging and relevant route of infection in potential bioterrorism attacks (*70, 71*). Mice were immunized with either iVAX- or PGCT-derived $MBP^{4xDQNAT}$, $PD^{4xDQNAT}$, or $EPA^{DNNNS\text{-}DQNRT}$ conjugates, as well as unmodified controls. Notably, across all three carrier proteins, only iVAX-derived vaccines elicited *Ft*O-PS-specific antibody titers that were significantly higher than those measured in the PBS immunized control group (**Figure 7b**). All immunized mice were challenged intranasally with 6000 cfu (60 times the intranasal LD_{50}) of the virulent *F. tularensis* subsp. *holarctica* LVS Rocky Mountain Laboratories. Importantly, all iVAX-derived vaccine candidates provided complete protection against intranasal challenge, which was indistinguishable from the protection conferred by PGCT-derived versions of the same vaccines (**Figure 7c-e**). These results demonstrate that the iVAX platform produces protective vaccine candidates that are at least as effective as those produced using a state-of-the-art biomanufacturing approach.

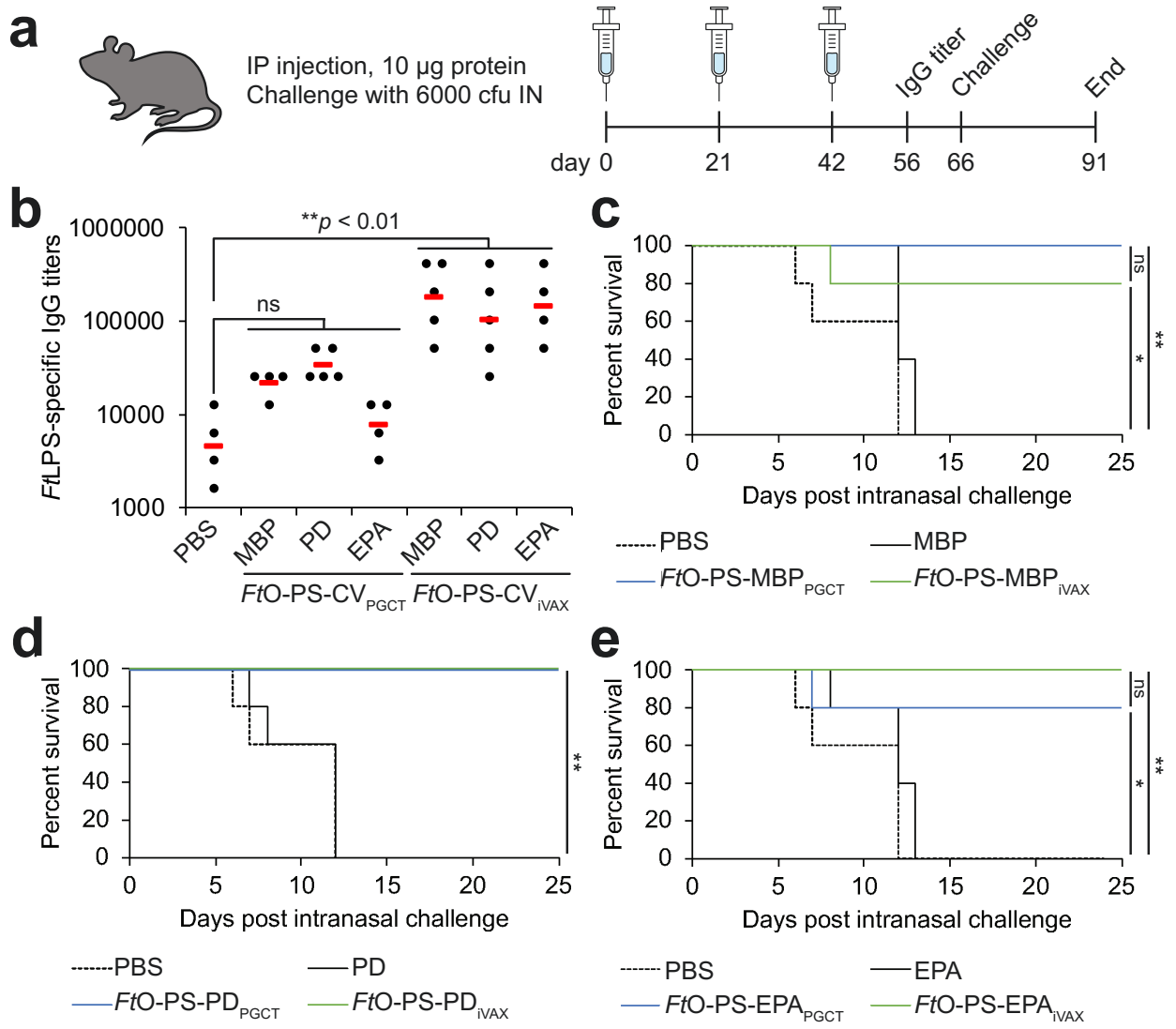

Figure 7. iVAX-derived conjugates protect mice from lethal *F. tularensis* challenge. (**a**) Groups of five BALB/c mice were immunized intraperitoneally with PBS or 10 µg of purified, cell-free synthesized unmodified or *Ft*O-PS-conjugated carrier proteins. *Ft*O-PS-conjugated carriers prepared in living *E. coli* cells using PCGT were used as positive controls. Mice were boosted on days 21 and 42 with identical doses of antigen. (**b**) On day 56, *Ft*LPS-specific IgG titers were measured by ELISA in serum of individual mice immunized with PBS or anti-*F. tularensis* conjugate vaccines (*Ft*O-PS-CV) (black dots) with *F. tularensis* LPS immobilized as antigen. Mean titers of each group are also shown (red lines). Only iVAX-derived conjugates elicited significantly higher levels of *Ft*LPS-specific IgG compared to PBS immunized controls across all carrier proteins tested (**$p < 0.01$, Tukey-Kramer HSD; CV: conjugate vaccine; ns: not significant). On day 66 mice were challenged intranasally with 6000 cfu (60 times the intranasal LD_{50}) *F. tularensis* subsp. *holarctica* LVS Rocky Mountain Laboratories and monitored for survival for an additional 25 days. Kaplan-Meier curves for immunizations with (**c**) $MBP^{4xDQNAT}$ (**d**) $PD^{4xDQNAT}$ and (**e**) $EPA^{DNNNS-DQNRT}$ as the carrier protein are shown. iVAX-derived vaccines protected mice from lethal pathogen challenge as effectively as vaccines synthesized using the state-of-the-art PGCT approach. (*$p < 0.05$; **$p < 0.01$, Fisher's exact test; ns: not significant).

Discussion

In this work we have established iVAX, a cell-free platform for portable, on-demand, and scalable production of protective conjugate vaccines. We show that iVAX reactions can be detoxified to ensure the safety of conjugate vaccine products, freeze-dried for cold chain-independent distribution, and re-activated for high-yielding conjugate production by simply adding water. As a model vaccine candidate, we show that anti-*F. tularensis* conjugates produced in iVAX elicited pathogen-specific IgG antibodies and protected mice from lethal intranasal challenge with *F. tularensis*. Given the proven impact of thermostable meningococcal and smallpox vaccines in reducing or eradicating disease (*24, 25*), iVAX has the potential to significantly enhance vaccination efforts by reducing reliance on refrigerated supply chains.

The iVAX platform has several important features. First, iVAX is modular, which we have demonstrated through the interchangeability of (i) carrier proteins, including those used in licensed conjugate vaccines, and (ii) bacterial O-PS antigens from *F. tularensis* subsp. *tularensis* (type A) Schu S4, ETEC E. coli O78, and UPEC E. coli O7. Importantly, iVAX is the first example of enrichment of large and polymeric *O*-antigen carbohydrates as substrates for cell-free protein glycosylation. Moreover, to our knowledge, this work represents the first demonstration of oligosaccharyltransferase-mediated O-PS conjugation to the carrier proteins used in licensed conjugate vaccine formulations, likely due to historical challenges associated with the expression of approved carriers in living *E. coli* (*31-33*). The modularity of iVAX has the potential to enable rapid development of conjugate vaccines against diverse bacteria as well as multiple serotypes of a single bacterial pathogen that can be co-formulated to yield multivalent conjugate vaccines. Further, iVAX could accelerate efforts to develop new carrier proteins that address issues related to carrier-induced epitopic suppression. Specifically, pre-existing immunity generated via DTaP and existing conjugate vaccines is known to diminish immune responses to bacterial polysaccharides conjugated to DT and TT (*50-53*). The modular iVAX platform promises to

facilitate production and evaluation of new carrier proteins in order to expand the repertoire of safe and effective conjugate vaccines that are compatible with pre-existing immunity within the population.

Second, iVAX reactions are inexpensive, costing ~$12 mL^{-1} (**table S1**) with the ability to synthesize ~20 μg conjugate mL^{-1} in one hour (**figure S4a**). Assuming a dose size of 10 μg, our iVAX reactions can produce a vaccine dose for ~$6. For comparison, the CDC cost per dose for conjugate vaccines ranges from ~$9.50 for the *H. influenzae* vaccine ActHIB® to ~$75 and ~$118 for the meningococcal vaccine Menactra® and pneumococcal vaccine Prevnar 13®, respectively (*72*).

Third, while conjugates derived from both living *E. coli* cells and iVAX PGCT protected mice from lethal challenge with *F. tularensis* LVS, iVAX-derived conjugates were significantly more effective at eliciting *Ft*LPS-specific IgGs than those derived from living *E. coli* cells using PGCT in the context of multiple carrier proteins (**Figure 6b, e**). Achieving high titers of polysaccharide-specific antibodies is broadly recognized as a correlate of conjugate vaccine efficacy (*20-23, 50-56*). Given the importance of antibodies in protection against infection with the highly virulent Schu S4 strain (*43, 44*), and the fact that antibody titers wane over time, achieving higher initial titers of *Ft*LPS-specific IgGs could provide protection against higher doses of pathogen and/or extend the duration of protection afforded by vaccination. Future comparative studies of iVAX- and PGCT-derived vaccines could provide a deeper understanding of immunogen features responsible for the enhanced *Ft*LPS-specific IgGs elicited by iVAX-derived vaccines, revealing design rules for the production of more effective conjugate vaccines.

Fourth, iVAX addresses a key gap in both cell-free and decentralized biomanufacturing technologies. Production of glycosylated products has not yet been demonstrated in cell-based decentralized biomanufacturing platforms (*73, 74*) and existing cell-free platforms using *E. coli* lysates lack the ability to synthesize glycoproteins (*28, 75-77*). While glycosylated human erythropoietin has been produced in a cell-free biomanufacturing platform based on freeze-dried

Chinese hamster ovary cell lysates, its *in vivo* efficacy was not evaluated and challenges achieving efficient glycosylation were noted (*29*). Further, this and the vast majority of other eukaryotic cell-free and cell-based systems rely on endogenous protein glycosylation machinery, and so are not compatible with conjugation of bacterial O-PS antigens. In contrast, the iVAX platform is enabled by our previous work to activate glycosylation in *E. coli* lysates that lack endogenous protein glycosylation pathways, which allows for bottom-up engineering of desired glycosylation activities (*37*). Here, we show that further development of this approach allows for rapid and portable production of protective conjugate vaccines. This required: (i) demonstration of modular cell-free synthesis and glycosylation of approved carrier proteins with O-PS antigens over a range of temperatures; (ii) rigorous assessment of reproducibility, scalability, and thermostability of reactions; (iii) detoxification of cell-free lysates; and (iv) evaluation of *in vivo* conjugate vaccine efficacy.

In summary, iVAX represents a platform technology for rapid development and on-demand, cold chain-independent biomanufacturing of conjugate vaccines. Conjugate vaccines are one of the safest and most effective methods for preventing bacterial infections (*2-4*), but their development and distribution is limited by current manufacturing approaches. The iVAX platform addresses these limitations and further provides the first example, to our knowledge, of efficacious glycoprotein product synthesis in a decentralized manufacturing platform. iVAX joins an emerging set of technologies (*28, 29, 73-77*) that have the potential to promote increased access to complex, life-saving drugs through decentralized production.

Acknowledgements

This work was supported by Defense Threat Reduction Agency (HDTRA1-15-10052/P00001 to M.P.D. and M.C.J.), National Science Foundation (Grants # CBET 1159581 and CBET 1264701

both to M.P.D. and MCB 1413563 to M.P.D. and M.C.J.), the Bill and Melinda Gates Foundation (OPP1217652 to M.P.D. and M.C.J.), the David and Lucile Packard Foundation, and the Dreyfus Teacher-Scholar program. J.C.S. and T.C.S. were supported by National Science Foundation Graduate Research Fellowships. T.J. was supported by a Royal Thai Government Fellowship. R.S.D. was funded, in part, by the Northwestern University Chemistry of Life Processes Summer Scholars program.

Author Contributions

J.C.S. and T.J. designed research, performed research, analyzed data, and wrote the paper. T.M. designed research, performed research, and analyzed data. J.M.H., K.F.W., B.S.M., A.M.M., R.S.D., and K.J.H. performed research. T.C.S. aided in research design. B.D.J. directed research. M.C.J. and M.P.D. directed research, analyzed data, and wrote the paper.

Declaration of Interests

M.P.D. has a financial interest in Glycobia, Inc. and Versatope, Inc. M.P.D. and M.C.J. have a financial interest in SwiftScale Biologics. M.P.D.'s and M.C.J.'s interests are reviewed and managed by Cornell University and Northwestern University, respectively, in accordance with their conflict of interest policies. All other authors declare no competing financial interests.

References and Notes

1. The Review on Antimicrobial Resistance, Antimicrobial Resistance: Tackling a crisis for the health and wealth of nations. (2014).

2. A. Weintraub, Immunology of bacterial polysaccharide antigens. *Carbohydr Res* **338**, 2539-2547 (2003).

3. C. L. Trotter *et al.*, Optimising the use of conjugate vaccines to prevent disease caused by Haemophilus influenzae type b, Neisseria meningitidis and Streptococcus pneumoniae. *Vaccine* **26**, 4434-4445 (2008).

4. C. Jin *et al.*, Efficacy and immunogenicity of a Vi-tetanus toxoid conjugate vaccine in the prevention of typhoid fever using a controlled human infection model of Salmonella Typhi: a randomised controlled, phase 2b trial. *Lancet* **390**, 2472-2480 (2017).

5. R. T. Novak *et al.*, Serogroup A meningococcal conjugate vaccination in Burkina Faso: analysis of national surveillance data. *Lancet Infect Dis* **12**, 757-764 (2012).

6. K. A. Poehling *et al.*, Invasive pneumococcal disease among infants before and after introduction of pneumococcal conjugate vaccine. *JAMA* **295**, 1668-1674 (2006).

7. S. W. Roush, L. McIntyre, L. M. Baldy, Manual for the surveillance of vaccine-preventable diseases. *Atlanta: Centers for Disease Control and Prevention*, 4 (2008).

8. B. Wahl *et al.*, Burden of Streptococcus pneumoniae and Haemophilus influenzae type b disease in children in the era of conjugate vaccines: global, regional, and national estimates for 2000-15. *Lancet Glob Health* **6**, e744-e757 (2018).

9. R. Bhushan, B. F. Anthony, C. E. Frasch, Estimation of group B streptococcus type III polysaccharide-specific antibody concentrations in human sera is antigen dependent. *Infect Immun* **66**, 5848-5853 (1998).

10. M. F. Feldman *et al.*, Engineering N-linked protein glycosylation with diverse O antigen lipopolysaccharide structures in Escherichia coli. *Proc Natl Acad Sci U S A* **102**, 3016-3021 (2005).

11. F. Garcia-Quintanilla, J. A. Iwashkiw, N. L. Price, C. Stratilo, M. F. Feldman, Production of a recombinant vaccine candidate against Burkholderia pseudomallei exploiting the bacterial N-glycosylation machinery. *Front Microbiol* **5**, 381 (2014).

12. M. Wetter *et al.*, Engineering, conjugation, and immunogenicity assessment of Escherichia coli O121 O antigen for its potential use as a typhoid vaccine component. *Glycoconj J* **30**, 511-522 (2013).

13. Z. Ma *et al.*, Glycoconjugate vaccine containing Escherichia coli O157:H7 O-antigen linked with maltose-binding protein elicits humoral and cellular responses. *PLoS One* **9**, e105215 (2014).

14. J. Cuccui *et al.*, Exploitation of bacterial N-linked glycosylation to develop a novel recombinant glycoconjugate vaccine against Francisella tularensis. *Open Biol* **3**, 130002 (2013).

15. L. E. Marshall *et al.*, An O-antigen glycoconjugate vaccine produced using protein glycan coupling technology is protective in an inhalational rat model of tularemia. *J Immunol Res* **2018**, 8087916 (2018).

16. M. Wacker *et al.*, Prevention of Staphylococcus aureus infections by glycoprotein vaccines synthesized in Escherichia coli. *J Infect Dis* **209**, 1551-1561 (2014).

17. J. Ihssen *et al.*, Production of glycoprotein vaccines in Escherichia coli. *Microb Cell Fact* **9**, 61 (2010).

18. C. E. Frasch, Preparation of bacterial polysaccharide-protein conjugates: analytical and manufacturing challenges. *Vaccine* **27**, 6468-6470 (2009).

19. WHO. Temperature sensitivity of vaccines. (2014).

20. F. Gao, K. Lockyer, K. Burkin, D. T. Crane, B. Bolgiano, A physico-chemical assessment of the thermal stability of pneumococcal conjugate vaccine components. *Hum Vaccin Immunother* **10**, 2744-2753 (2014).

21. N. J. Beresford *et al.*, Quality, immunogenicity and stability of meningococcal serogroup ACWY-CRM(197), DT and TT glycoconjugate vaccines. *Vaccine* **35**, 3598-3606 (2017).

22. M. M. Ho *et al.*, Physico-chemical and immunological examination of the thermal stability of tetanus toxoid conjugate vaccines. *Vaccine* **20**, 3509-3522 (2002).

23. M. M. Ho, B. Bolgiano, M. J. Corbel, Assessment of the stability and immunogenicity of meningococcal oligosaccharide C-CRM197 conjugate vaccines. *Vaccine* **19**, 716-725 (2000).

24. J. W. Hopkins, The eradication of smallpox: organizational learning and innovation in international health administration. *J Dev Areas* **22**, 321-332 (1988).

25. P. Lydon *et al.*, Economic benefits of keeping vaccines at ambient temperature during mass vaccination: the case of meningitis A vaccine in Chad. *Bull World Health Organ* **92**, 86-92 (2014).

26. A. Ashok, M. Brison, Y. LeTallec, Improving cold chain systems: Challenges and solutions. *Vaccine* **35**, 2217-2223 (2017).

27. A. D. Silverman, A. S. Karim, M. C. Jewett, Cell-free gene expression: an expanded repertoire of applications. *Nat Rev Genet* **21**, 151-170 (2020).

28. K. Pardee *et al.*, Portable, on-demand biomolecular manufacturing. *Cell* **167**, 248-259.e212 (2016).

29. R. Adiga *et al.*, Point-of-care production of therapeutic proteins of good-manufacturing-practice quality. *Nat Biomed Eng*, (2018).

30. N. Sethuraman, T. A. Stadheim, Challenges in therapeutic glycoprotein production. *Curr. Opin. Biotechnol.* **17**, 341-346 (2006).

31. F. Haghi, S. N. Peerayeh, S. D. Siadat, M. Montajabiniat, Cloning, expression and purification of outer membrane protein PorA of Neisseria meningitidis serogroup B. *J Infect Dev Ctries* **5**, 856-862 (2011).

32. A. Stefan *et al.*, Overexpression and purification of the recombinant diphtheria toxin variant CRM197 in Escherichia coli. *J Biotechnol* **156**, 245-252 (2011).

33. D. Figueiredo *et al.*, Characterization of recombinant tetanus toxin derivatives suitable for vaccine development. *Infect Immun* **63**, 3218-3221 (1995).

34. J. G. Perez, J. C. Stark, M. C. Jewett, Cell-free synthetic biology: Engineering beyond the cell. *Cold Spring Harb Perspect Biol*, (2016).

35. S. Fernandez *et al.*, Potential role for Toll-like receptor 4 in mediating Escherichia coli maltose-binding protein activation of dendritic cells. *Infect Immun* **75**, 1359-1363 (2007).

36. M. M. Chen, K. J. Glover, B. Imperiali, From peptide to protein: comparative analysis of the substrate specificity of N-linked glycosylation in C. jejuni. *Biochemistry* **46**, 5579-5585 (2007).

37. T. Jaroentomeechai *et al.*, Single-pot glycoprotein biosynthesis using a cell-free transcription-translation system enriched with glycosylation machinery. *Nat Commun* **9**, 2686 (2018).

38. T. H. Bayburt, S. G. Sligar, Membrane protein assembly into Nanodiscs. *FEBS Lett* **584**, 1721-1727 (2010).

39. D. M. Kim, J. R. Swartz, Efficient production of a bioactive, multiple disulfide-bonded protein using modified extracts of Escherichia coli. *Biotechnol Bioeng* **85**, 122-129 (2004).

40. P. C. Oyston, A. Sjostedt, R. W. Titball, Tularaemia: bioterrorism defence renews interest in Francisella tularensis. *Nat Rev Microbiol* **2**, 967-978 (2004).

41. M. Maurin, Francisella tularensis as a potential agent of bioterrorism? *Expert Rev Anti Infect Ther* **13**, 141-144 (2015).

42. CDC. Ring vaccination (2019).

43. M. Fulop, P. Mastroeni, M. Green, R. W. Titball, Role of antibody to lipopolysaccharide in protection against low- and high-virulence strains of Francisella tularensis. *Vaccine* **19**, 4465-4472 (2001).

44. Z. Lu *et al.*, Protective B-cell epitopes of Francisella tularensis O-polysaccharide in a mouse model of respiratory tularaemia. *Immunology* **136**, 352-360 (2012).

45. J. L. Prior *et al.*, Characterization of the O antigen gene cluster and structural analysis of the O antigen of Francisella tularensis subsp. tularensis. *J Med Microbiol* **52**, 845-851 (2003).

46. L. Chen *et al.*, Outer membrane vesicles displaying engineered glycotopes elicit protective antibodies. *Proc Natl Acad Sci U S A* (2016).

47. M. Kowarik *et al.*, Definition of the bacterial N-glycosylation site consensus sequence. *EMBO J* **25**, 1957-1966 (2006).

48. A. A. Palmu *et al.*, Effectiveness of the ten-valent pneumococcal Haemophilus influenzae protein D conjugate vaccine (PHiD-CV10) against invasive pneumococcal disease: a cluster randomised trial. *Lancet* **381**, 214-222 (2013).

49. S. A. Silfverdal *et al.*, Immunogenicity of a 2-dose priming and booster vaccination with the 10-valent pneumococcal nontypeable Haemophilus influenzae protein D conjugate vaccine. *Pediatr Infect Dis J* **28**, e276-282 (2009).

50. R. Dagan, J. Eskola, C. Leclerc, O. Leroy, Reduced response to multiple vaccines sharing common protein epitopes that are administered simultaneously to infants. *Infect Immun* **66**, 2093-2098 (1998).

51. M. Burrage *et al.*, Effect of vaccination with carrier protein on response to meningococcal C conjugate vaccines and value of different immunoassays as predictors of protection. *Infect Immun* **70**, 4946-4954 (2002).

52. R. Dagan, D. Goldblatt, J. R. Maleckar, M. Yaïch, J. Eskola, Reduction of antibody response to an 11-valent pneumococcal vaccine coadministered with a vaccine containing acellular pertussis components. *Infect Immun* **72**, 5383-5391 (2004).

53. M. Knuf *et al.*, Immunogenicity of routinely used childhood vaccines when coadministered with the 10-valent pneumococcal non-typeable Haemophilus influenzae protein D conjugate vaccine (PHiD-CV). *Pediatr Infect Dis J* **28**, S97-s108 (2009).

54. C. F. Hatz *et al.*, Safety and immunogenicity of a candidate bioconjugate vaccine against Shigella dysenteriae type 1 administered to healthy adults: A single blind, partially randomized Phase I study. *Vaccine* **33**, 4594-4601 (2015).

55. A. Huttner *et al.*, Safety, immunogenicity, and preliminary clinical efficacy of a vaccine against extraintestinal pathogenic Escherichia coli in women with a history of recurrent urinary tract infection: a randomised, single-blind, placebo-controlled phase 1b trial. *Lancet Infect Dis*, (2017).

56. M. S. Riddle *et al.*, Safety and immunogenicity of a candidate bioconjugate vaccine against Shigella flexneri 2a administered to healthy adults: a single blind, randomized phase I study. *Clin Vaccine Immunol*, (2016).

57. G. Humphreys. (World Health Organization, Bulletin of the World Health Organization, 2011).

58. F. Qadri, A. M. Svennerholm, A. S. Faruque, R. B. Sack, Enterotoxigenic Escherichia coli in developing countries: epidemiology, microbiology, clinical features, treatment, and prevention. *Clin Microbiol Rev* **18**, 465-483 (2005).

59. J. R. Johnson, Virulence factors in Escherichia coli urinary tract infection. *Clin Microbiol Rev* **4**, 80-128 (1991).

60. P. E. Jansson, B. Lindberg, G. Widmalm, K. Leontein, Structural studies of the Escherichia coli O78 O-antigen polysaccharide. *Carbohydr Res* **165**, 87-92 (1987).

61. V. L. L'vov *et al.*, Structural studies of the O-specific side chain of the lipopolysaccharide from Escherichia coli O:7. *Carbohydr Res* **126**, 249-259 (1984).

62. J. A. Russell, Management of sepsis. *N Engl J Med* **355**, 1699-1713 (2006).

63. L. A. Brito, M. Singh, Acceptable levels of endotoxin in vaccine formulations during preclinical research. *J Pharm Sci* **100**, 34-37 (2011).

64. D. Petsch, F. B. Anspach, Endotoxin removal from protein solutions. *J Biotechnol* **76**, 97-119 (2000).

65. B. D. Needham *et al.*, Modulating the innate immune response by combinatorial engineering of endotoxin. *Proc Natl Acad Sci U S A* **110**, 1464-1469 (2013).

66. C. R. Casella, T. C. Mitchell, Putting endotoxin to work for us: monophosphoryl lipid A as a safe and effective vaccine adjuvant. *Cell Mol Life Sci* **65**, 3231-3240 (2008).

67. B. Bolgiano *et al.*, A retrospective study on the quality of Haemophilus influenzae type b vaccines used in the UK between 1996 and 2004. *Hum Vaccin* **3**, 176-182 (2007).

68. D. Bogaert, P. W. Hermans, P. V. Adrian, H. C. Rumke, R. de Groot, Pneumococcal vaccines: an update on current strategies. *Vaccine* **22**, 2209-2220 (2004).

69. G. Stefanetti, N. Okan, A. Fink, E. Gardner, D. L. Kasper, Glycoconjugate vaccine using a genetically modified O antigen induces protective antibodies to Francisella tularensis. *Proc Natl Acad Sci U S A* **116**, 7062-7070 (2019).

70. J. W. Conlan, H. Shen, A. Webb, M. B. Perry, Mice vaccinated with the O-antigen of Francisella tularensis LVS lipopolysaccharide conjugated to bovine serum albumin develop varying degrees of protective immunity against systemic or aerosol challenge with virulent type A and type B strains of the pathogen. *Vaccine* **20**, 3465-3471 (2002).

71. S. Sebastian *et al.*, Cellular and humoral immunity are synergistic in protection against types A and B Francisella tularensis. *Vaccine* **27**, 597-605 (2009).

72. CDC, CDC Vaccine Price List. (2019).

73. L. E. Crowell *et al.*, On-demand manufacturing of clinical-quality biopharmaceuticals. *Nat Biotechnol*, (2018).

74. P. Perez-Pinera *et al.*, Synthetic biology and microbioreactor platforms for programmable production of biologics at the point-of-care. *Nat Commun* **7**, 12211 (2016).

75. A. S. Salehi *et al.*, Cell-free protein synthesis of a cytotoxic cancer therapeutic: Onconase production and a just-add-water cell-free system. *Biotechnol J* **11**, 274-281 (2016).

76. T. W. Murphy, J. Sheng, L. B. Naler, X. Feng, C. Lu, On-chip manufacturing of synthetic proteins for point-of-care therapeutics. *Microsyst Nanoeng* **5**, 13 (2019).

77. K. S. Boles *et al.*, Digital-to-biological converter for on-demand production of biologics. *Nat Biotechnol* **35**, 672-675 (2017).

78. A. C. Fisher *et al.*, Production of secretory and extracellular N-linked glycoproteins in Escherichia coli. *Appl Environ Microbiol* **77**, 871-881 (2011).

79. K. A. Datsenko, B. L. Wanner, One-step inactivation of chromosomal genes in Escherichia coli K-12 using PCR products. *Proc Natl Acad Sci U S A* **97**, 6640-6645 (2000).

80. A. A. Ollis *et al.*, Substitute sweeteners: Diverse bacterial oligosaccharyltransferases with unique N-glycosylation site preferences. *Sci Rep* **5**, 15237 (2015).

81. M. C. Jewett, J. R. Swartz, Mimicking the Escherichia coli cytoplasmic environment activates long-lived and efficient cell-free protein synthesis. *Biotechnol Bioeng* **86**, 19-26 (2004).

82. J. A. Schoborg *et al.*, A cell-free platform for rapid synthesis and testing of active oligosaccharyltransferases. *Biotechnol Bioeng*, (2017).

83. D. J. Chen *et al.*, Delivery of foreign antigens by engineered outer membrane vesicle vaccines. *Proc Natl Acad Sci U S A* **107**, 3099-3104 (2010).

84. S. H. Hong *et al.*, Cell-free protein synthesis from a release factor 1 deficient Escherichia coli activates efficient and multiple site-specific nonstandard amino acid incorporation. *ACS Synth Biol* **3**, 398-409 (2014).

85. D. M. Kim, J. R. Swartz, Regeneration of adenosine triphosphate from glycolytic intermediates for cell-free protein synthesis. *Biotechnol Bioeng* **74**, 309-316 (2001).

86. A. A. Ollis, S. Zhang, A. C. Fisher, M. P. DeLisa, Engineered oligosaccharyltransferases with greatly relaxed acceptor-site specificity. *Nat Chem Biol* **10**, 816-822 (2014).

87. E. Celik *et al.*, Glycoarrays with engineered phages displaying structurally diverse oligosaccharides enable high-throughput detection of glycan-protein interactions. *Biotechnol J* **10**, 199-209 (2015).

88. M. A. Valvano, J. H. Crosa, Molecular cloning and expression in Escherichia coli K-12 of chromosomal genes determining the O7 lipopolysaccharide antigen of a human invasive strain of E. coli O7:K1. *Infect Immun* **57**, 937-943 (1989).

List of Supplementary Materials

Materials and Methods
Fig S1-S7
Table S1-S4
References 64-73

Science
AAAS

Supplementary Materials for

On-demand biomanufacturing of protective conjugate vaccines

Jessica C. Stark, † Thapakorn Jaroentomeechai, † Tyler D. Moeller, Jasmine M. Hershewe, Katherine F. Warfel, Bridget S. Moricz, Anthony M. Martini, Rachel S. Dubner, Karen J. Hsu, Taylor C. Stevenson, Bradley D. Jones, Matthew P. DeLisa, and Michael C. Jewett

† J.C.S. and T. J. contributed equally
Correspondence to: m-jewett@northwestern.edu & md255@cornell.edu

This PDF file includes:

Materials and Methods

Bacterial strains and plasmids

E. coli NEB 5-alpha (NEB) was used for plasmid cloning and purification. *E. coli* CLM24 or CLM24 Δ*lpxM* strains were used for preparing cell-free lysates. *E. coli* CLM24 was used as the chassis for expressing conjugates *in vivo* using PGCT. As a derivative of the W3110 *E. coli* K strain, CLM24 does not synthesize an endogenous O-PS antigen due to an inactivating mutation in the gene encoding the WbbL O-PS glycosyltransferase, enabling unimpeded biosynthesis of heterologous O-PS antigens on undecaprenyl diphosphate (UndPP). CLM24 further has a deletion in the gene encoding the WaaL ligase that transfers O-PS antigens from UndPP to lipid A, facilitating the accumulation of preassembled glycans on UndPP as substrates for *Cj*PglB-mediated protein glycosylation (*1*). CLM24 Δ*lpxM* has an endogenous acyltransferase deletion and serves as the chassis strain for production of detoxified cell-free lysates.

All plasmids used in the study are listed in **table S2**. Plasmids pJL1-MBP^{4xDQNAT}, pJL1-PD^{4xDQNAT}, pJL1-PorA^{4xDQNAT}, pJL1-TTc^{4xDQNAT}, pJL1-TTlight^{4xDQNAT}, pJL1-CRM197^{4xDQNAT}, and pJL1-TT^{4xDQNAT} were generated via PCR amplification and subsequent Gibson Assembly of a codon optimized gene construct purchased from IDT with a C-terminal 4xDQNAT-6xHis tag (*2*) between the *NdeI* and *SalI* restriction sites in the pJL1 vector. Plasmid pJL1-EPA$^{DNNNS-DQNRT}$ was constructed using the same approach, but without the addition of a C-terminal 4xDQNAT-6xHis tag. Plasmids pTrc99s-ssDsbA-MBP^{4xDQNAT}, pTrc99s-ssDsbA-PD^{4xDQNAT}, pTrc99s-ssDsbA-PorA^{4xDQNAT}, pTrc99s-ssDsbA-TTc^{4xDQNAT}, pTrc99s-ssDsbA-TTlight^{4xDQNAT}, and pTrc99s-ssDsbA-EPA$^{DNNNS-DQNRT}$ were created via PCR amplification of each carrier protein gene and insertion into the pTrc99s vector between the *NcoI* and *HindIII* restriction sites via Gibson Assembly. Plasmid pSF-*Cj*PglB-LpxE was constructed using a similar approach, but via insertion of the *lpxE* gene from pE (*3*) between the *NdeI* and *NsiI* restriction sites in the pSF vector. Inserts were amplified via PCR using Phusion® High-Fidelity DNA polymerase (NEB) with forward and reverse

primers designed using the NEBuilder® Assembly Tool (nebuilder.neb.com) and purchased from IDT. The pJL1 vector (Addgene 69496) was digested using restriction enzymes NdeI and SalI-HF® (NEB). The pSF vector was digested using restriction enzymes NdeI and NotI (NEB). PCR products were gel extracted using an EZNA Gel Extraction Kit (Omega Bio-Tek), mixed with Gibson assembly reagents and incubated at 50°C for 1 hour. Plasmid DNA from the Gibson assembly reactions were transformed into *E. coli* NEB 5-alpha cells and circularized constructs were selected using kanamycin at 50 μg ml^{-1} (Sigma). Sequence-verified clones were purified using an EZNA Plasmid Midi Kit (Omega Bio-Tek) for use in CFPS and iVAX reactions.

Construction of CLM24 ΔlpxM strain

E. coli CLM24 Δ*lpxM* was generated using the Datsenko-Wanner gene knockout method (*4*). Briefly, CLM24 cells were transformed with the pKD46 plasmid encoding the λ red system. Transformants were grown to an OD_{600} of 0.5-0.7 in 25 mL LB-Lennox media (10 g L^{-1} tryptone, 5 g L^{-1} yeast extract and 5 g L^{-1} NaCl) with 50 μg mL^{-1} carbenicillin at 30°C, harvested and washed three times with 25 mL ice-cold 10% glycerol to make them electrocompetent, and resuspended in a final volume of 100 μL 10% glycerol. In parallel, a *lpxM* knockout cassette was generated by PCR amplifying the kanamycin resistance cassette from pKD4 with forward and reverse primers with homology to *lpxM*. Electrocompetent cells were transformed with 400 ng of the *lpxM* knockout cassette and plated on LB agar with 30 μg mL^{-1} kanamycin for selection of resistant colonies. Plates were grown at 37°C to cure cells of the pKD46 plasmid. Colonies that grew on kanamycin were confirmed to have acquired the knockout cassette via colony PCR and DNA sequencing. These confirmed colonies were then transformed with pCP20 to remove the kanamycin resistance gene via Flp-FRT recombination. Transformants were plated on LB agar with 50 μg mL^{-1} carbenicillin. Following selection, colonies were grown in liquid culture at 42°C to cure cells of the pCP20 plasmid. Colonies were confirmed to have lost both *lpxM* and the knockout cassette via colony PCR and DNA sequencing and confirmed to have lost both kanamycin and carbenicillin

resistance via replica plating on LB agar plates with 50 μg mL^{-1} carbenicillin or kanamycin. All primers used for construction and validation of this strain are listed in **table S3**.

Cell-free lysate preparation

E. coli CLM24 source strains were grown in 2xYTP media (10 g/L yeast extract, 16 g/L tryptone, 5 g/L NaCl, 7 g/L K_2HPO_4, 3 g/L KH_2PO_4, pH 7.2) in shake flasks (1 L scale) or a Sartorius Stedim BIOSTAT Cplus bioreactor (10 L scale) at 37°C. To generate *Cj*PglB-enriched lysate, CLM24 cells carrying plasmid pSF-*Cj*PglB (*5*) was used as the source strain. To generate *Ft*O-PS-enriched lysates, CLM24 carrying plasmid pGAB2 (*6*) was used as the source strain. To generate one-pot lysates containing both *Cj*PglB and *Ft*O-PS, *Ec*O78-PS, or *Ec*O7-PS, CLM24 carrying pSF-*Cj*PglB and one of the following bacterial O-PS biosynthetic pathway plasmids was used as the source strain: pGAB2 (*Ft*O-PS), pMW07-O78 (*Ec*O78-PS), and pJHCV32 (*Ec*O7-PS). *Cj*PglB expression was induced at an OD_{600} of 0.8-1.0 with 0.02% (w/v) L-arabinose and cultures were moved to 30°C. Cells were grown to a final OD_{600} of ~3.0, at which point cells were pelleted by centrifugation at 5,000xg for 15 min at 4°C. Cell pellets were then washed three times with cold S30 buffer (10 mM Tris-acetate pH 8.2, 14 mM magnesium acetate, 60 mM potassium acetate) and pelleted at 5000xg for 10 min at 4°C. After the final wash, cells were pelleted at 7000xg for 10 min at 4°C, weighed, flash frozen in liquid nitrogen, and stored at -80°C. To make cell lysate, cell pellets were resuspended to homogeneity in 1 mL of S30 buffer per 1 g of wet cell mass. Cells were disrupted via a single passage through an Avestin EmulsiFlex-B15 (1 L scale) or EmulsiFlex-C3 (10 L scale) high-pressure homogenizer at 20,000-25,000 psi. The lysate was then centrifuged twice at 30,000×g for 30 min to remove cell debris. Supernatant was transferred to clean microcentrifuge tubes and incubated at 37°C with shaking at 250 rpm for 60 min. Following centrifugation (15,000xg) for 15 min at 4°C, supernatant was collected, aliquoted, flash-frozen in liquid nitrogen, and stored at -80°C. S30 lysate was active for about 3 freeze-thaw cycles and contained ~40 g/L total protein as measured by Bradford assay.

Cell-free protein synthesis

CFPS reactions were carried out in 1.5 mL microcentrifuge tubes (15 µL scale), 15 mL conical tubes (1 mL scale), or 50 mL conical tubes (5 mL scale) with a modified PANOx-SP system (*7*). The CFPS reaction mixture consists of the following components: 1.2 mM ATP; 0.85 mM each of GTP, UTP, and CTP; 34.0 µg mL^{-1} L-5-formyl-5, 6, 7, 8-tetrahydrofolic acid (folinic acid); 170.0 µg mL^{-1} of *E. coli* tRNA mixture; 130 mM potassium glutamate; 10 mM ammonium glutamate; 12 mM magnesium glutamate; 2 mM each of 20 amino acids; 0.4 mM nicotinamide adenine dinucleotide (NAD); 0.27 mM coenzyme-A (CoA); 1.5 mM spermidine; 1 mM putrescine; 4 mM sodium oxalate; 33 mM phosphoenolpyruvate (PEP); 57 mM HEPES; 13.3 µg mL^{-1} plasmid; and 27% v/v of cell lysate. For reaction volumes ≥1 mL, plasmid was added at 6.67 µg mL^{-1}, as this lower plasmid concentration conserved reagents with no effect on protein synthesis yields or kinetics. For expression of PorA, reactions were supplemented with nanodiscs at 1 µg mL^{-1}, which were prepared as previously described (*8*) or purchased (Cube Biotech). For expression of $CRM197^{4xDQNAT}$, CFPS was carried out at 25°C for 20 hours, unless otherwise noted. For all other carrier proteins, CFPS was run at 30°C for 20 hours, unless otherwise noted.

For expression of $TT^{4xDQNAT}$, which contains intermolecular disulfide bonds, CFPS was carried out under oxidizing conditions, as previously reported (*9*). For oxidizing conditions, lysate was pre-conditioned with 750 µM iodoacetamide at room temperature for 30 min to covalently bind free sulfhydryls (-SH), including the active site cysteines of the thioredoxin reductase (trxB) and glutathione reductase (gor) enzymes that represent the primary disulfide bond reducing enzymes in the *E. coli* cytoplasm. The CFPS reaction mix was then supplemented with 200 mM glutathione at a 4:1 ratio of oxidized and reduced forms and 10 µM recombinant *E. coli* DsbC (*9*).

In vitro conjugate vaccine expression (iVAX)

For *in vitro* expression and glycosylation of carrier proteins in crude lysates, a two-phase scheme was implemented. In the first phase, CFPS was carried out for 15 min at 25-30 °C as described above. In the second phase, protein glycosylation was initiated by the addition of $MnCl_2$ and DDM at a final concentration of 25 mM and 0.1% (w/v), respectively, and allowed to proceed at 30°C for a total reaction time of 1 hour. Reactions were then centrifuged at 20,000xg for 10 min to remove insoluble or aggregated protein products and the supernatant was analyzed by SDS-PAGE and Western blotting.

Purification of unmodified and O-PS-conjugated carriers from iVAX reactions was carried out using Ni-NTA agarose (Qiagen) according to manufacturer's protocols. Briefly, 0.5 mL Ni-NTA agarose per 1 mL cell-free reaction mixture was equilibrated in Buffer 1 (300 mM NaCl 50 mM NaH_2PO_4) with 10 mM imidazole. Soluble fractions from iVAX reactions were loaded on Ni-NTA agarose and incubated at 4°C for 2-4 hours to bind 6xHis-tagged protein. Following incubation, the cell-free reaction/agarose mixture was loaded onto a polypropylene column (BioRad) and washed twice with 6 column volumes of Buffer 1 with 20 mM imidazole. Protein was eluted in 4 fractions, each with 0.3 mL Buffer 1 with 300 mM imidazole per mL of cell-free reaction mixture. All buffers were used and stored at 4°C. Protein was stored at a final concentration of 1-2 mg mL^{-1} in sterile 1xPBS (137 mM NaCl, 2.7 mM KCl, 10 mM Na_2HPO_4, 1.8 mM KH_2PO_4, pH 7.4) at 4°C.

Lyophilization of iVAX reactions

iVAX reactions were prepared according to the recipe above and lyophilized using a VirTis BenchTop Pro lyophilizer (SP Scientific) at 100 mTorr and −80 °C overnight or until fully freeze-dried. Following lyophilization, freeze-dried pellets were rehydrated with nuclease-free water (Ambion) and run as described above. If reactions were stored at ambient temperature after lyohilization, they were stored under vacuum using economic packaging materials. Specifically, we vacuum sealed reactions using a commercial FoodSaver® appliance with Dri-Card™ desiccant cards enclosed to prevent rehydration of the iVAX pellets. Our results show that freeze-dried iVAX

pellets can be stored at ambient temperature for up to 3 months with no loss of activity (**figure S7**).

Expression of conjugates in vivo using protein glycan coupling technology (PGCT)

Plasmids encoding conjugate carrier protein genes preceded by the DsbA leader sequence for translocation to the periplasm were transformed into CLM24 cells carrying pGAB2 and pSF-*Cj*PglB. CLM24 carrying only pGAB2 was used as a negative control. Transformed cells were grown in 5 mL LB media (10 g L^{-1} yeast extract, 5 g L^{-1} tryptone, 5 g L^{-1} NaCl) overnight at 37°C. The next day, cells were subcultured into 100 mL LB and allowed to grow at 37°C for 6 hours after which the culture was supplemented with 0.2% arabinose and 0.5 mM IPTG to induce expression of *Cj*PglB and the conjugate carrier protein, respectively. Protein expression was then carried out for 16 hours at 30°C, at which point cells were harvested. Cell pellets were resuspended in 1 mL sterile PBS (137 mM NaCl, 2.7 mM KCl, 10 mM Na_2HPO_4, 1.8 mM KH_2PO_4, pH 7.4) and lysed using a Q125 Sonicator (Qsonica, Newtown, CT) at 40% amplitude in cycles of 10 sec on/10 sec off for a total of 5 min. Soluble fractions were isolated following centrifugation at 15,000 rpm for 30 min at 4°C. Protein was purified from soluble fractions using Ni-NTA spin columns (Qiagen), following the manufacturer's protocol.

Western blot analysis

Samples were run on 4-12% Bis-Tris SDS-PAGE gels (Invitrogen). Following electrophoretic separation, proteins were transferred from gels onto Immobilon-P polyvinylidene difluoride (PVDF) membranes (0.45 µm) according to the manufacturer's protocol. Membranes were washed with PBS (80 g L^{-1} NaCl, 0.2 g L^{-1} KCl, 1.44 g L^{-1} Na_2HPO_4, 0.24 g L^{-1} KH_2PO_4, pH 7.4) followed by incubation for 1 hour in Odyssey® Blocking Buffer (LI-COR). After blocking, membranes were washed 6 times with PBST (80 g L^{-1} NaCl, 0.2 g L^{-1} KCl, 1.44 g L^{-1} Na_2HPO_4, 0.24 g L^{-1} KH_2PO_4, 1 mL L^{-1} Tween-20, pH 7.4) with a 5 min incubation between each wash. For

iVAX samples, membranes were probed with both an anti-6xHis tag antibody and an anti-O-PS antibody or antisera specific to the O antigen of interest, if commercially available. Probing of membranes was performed for at least 1 hour with shaking at room temperature, after which membranes were washed with PBST in the same manner as described above and probed with fluorescently labeled secondary antibodies. Membranes were imaged using an Odyssey® Fc imaging system (LI-COR). CRM197 and TT production were compared to commercial DT and TT standards (Sigma) and orthogonally detected by an identical SDS-PAGE procedure followed by Western blot analysis with a polyclonal antibody that recognizes diphtheria or tetanus toxin, respectively. All antibodies and dilutions used are listed in **table S4**.

TLR4 activation assay

HEK-Blue hTLR4 cells (Invivogen) were cultured in DMEM media, high glucose/L-glutamine supplement with 10% fetal bovine serum, 50 U mL^{-1} penicillin, 50 mg mL^{-1} streptomycin, and 100 µg mL^{-1} Normacin™ at 37ºC in a humidified incubator containing 5% CO_2. After reaching ~50-80% confluency, cells were plated into 96-well plates at a density of 1.4×10^5 cells per mL in HEK-Blue detection media (Invivogen). Antigens were added at the following concentrations: 100 ng $µL^{-1}$ purified protein; and 100 ng $µL^{-1}$ total protein in lysate. Purified *E. coli* O55:B5 LPS (Sigma-Aldrich) and detoxified *E. coli* O55:B5 (Sigma-Aldrich) were added at 1.0 ng mL^{-1} and served as positive and negative controls, respectively. Plates were incubated at 37°C, 5% CO_2 for 10–16 h before measuring absorbance at 620 nm. Statistical significance was determined using paired *t*-tests.

Mouse immunization and F. tularensis challenge

Groups of 5-6 six-week old female BALB/c mice (Harlan Sprague Dawley) were immunized with 100 µL PBS (pH 7.4) alone or containing purified MBP, *Ft*O-PS-conjugated MBP, PD, *Ft*O-PS-conjugated PD, EPA, or *Ft*O-PS-conjugated EPA, as previously described (*10*). The amount of

antigen in each preparation was normalized to ensure that an equivalent amount of unmodified protein or conjugate was administered in each case. Purified protein groups formulated in PBS were mixed with an equal volume of incomplete Freund's Adjuvant (Sigma-Aldrich) before injection. Prior to immunization, material for each group (5 μL) was streaked on LB agar plates and grown overnight at 37°C to confirm sterility and endotoxin activity was measured by TLR4 activation assay. Each group of mice was boosted with an identical dosage of antigen 21 days and 42 days after the initial immunization. Mice were observed 24 and 48 hours after each injection for changes in behavior and physical health and no abnormal responses were reported.

For initial antibody titering studies, mice were immunized subcutaneously with 7.5 μg vaccine or controls according to the protocol described above. Blood was obtained on day -1, 21, 35, 49, and 63 via submandibular collection and at study termination on day 70 via cardiac puncture.

For pathogen challenge studies, mice were immunized intraperitoneally with to 10 μg vaccine or controls according to the protocol described above. Blood for antibody titering was obtained on day 56 via submandibular collection. Mice were challenged intranasally on day 66 with 6000 cfu (60 times the intranasal LD_{50}) *F. tularensis* subsp. *holarctica* LVS Rocky Mountain Laboratories. Survival was monitored for an additional 25 days following pathogen challenge, during which mice were examined daily for signs of disease and sacrificed according to the approved protocol when moribund. Statistical significance was determined via endpoint comparison using Fisher's exact test.

All procedures were carried out in accordance with Protocol 2012-0132 approved by the Cornell University Institutional Animal Care and Use Committee and/or Protocol 1305086 approved by the University of Iowa Animal Care and Use Committee.

Enzyme-linked immunosorbent assay

F. tularensis LPS-specific antibodies elicited by immunized mice were measured via indirect ELISA using a modification of a previously described protocol (*10*). Briefly, sera were isolated from the collected blood draws after centrifugation at 5000xg for 10 min and stored at −20 °C; 96-well plates (Maxisorp; Nunc Nalgene) were coated with *F. tularensis* LPS (BEI resources) at a concentration of 5 μg mL^{-1} in PBS and incubated overnight at 4°C. The next day, plates were washed three times with PBST (PBS, 0.05% Tween-20, 0.3% BSA) and blocked overnight at 4°C with 5% nonfat dry milk (Carnation) in PBS. Samples were serially diluted by a factor of two in triplicate between 1:100 and 1:12,800,000 in blocking buffer and added to the plate for 2 hours at 37°C. Plates were washed three times with PBST and incubated for 1 hour at 37°C in the presence of one of the following HRP-conjugated antibodies (all from Abcam and used at 1:25,000 dilution): goat anti-mouse IgG, anti-mouse IgG1, and anti-mouse IgG2a. After three additional washes with PBST, 3,3′-5,5′-tetramethylbenzidine substrate (1-Step Ultra TMB-ELISA; Thermo-Fisher) was added, and the plate was incubated at room temperature in the dark for 30 min. The reaction was halted with 2 M H_2SO_4, and absorbance was quantified via microplate spectrophotometer (Tecan) at a wavelength of 450 nm. Serum antibody titers were determined by measuring the lowest dilution that resulted in signal 3 SDs above no serum background controls. Statistical significance was determined in RStudio 1.1.463 using one-way ANOVA and the Tukey–Kramer *post hoc* honest significant difference test.

Quantification and Statistical Analysis

Quantification of cell-free protein synthesis yields and autoradiography

To quantify the amount of protein synthesized in iVAX reactions, two approaches were used. Fluorescence units of sfGFP were converted to concentrations using a previously reported standard curve (*11*). Yields of all other proteins were assessed via the addition of 10 μM L-^{14}C-leucine (11.1 GBq $mmol^{-1}$, PerkinElmer) to the CFPS mixture to yield trichloroacetic acid-precipitable radioactivity that was measured using a liquid scintillation counter as described

previously (*12*). Soluble fractions were also run on an SDS-PAGE gel and exposed by autoradiography. Autoradiographs were imaged with a Typhoon 7000 (GE Healthcare Life Sciences).

Statistical analysis

Statistical parameters including the definitions and values of *n*, *p*-values, standard deviations, and standard errors are reported in the figures and corresponding figure legends. Analytical techniques are described in the corresponding Materials and Methods section.

Data and Software Availability

All plasmid constructs used in this study including complete DNA sequences are deposited on Addgene (constructs 128389-128404).

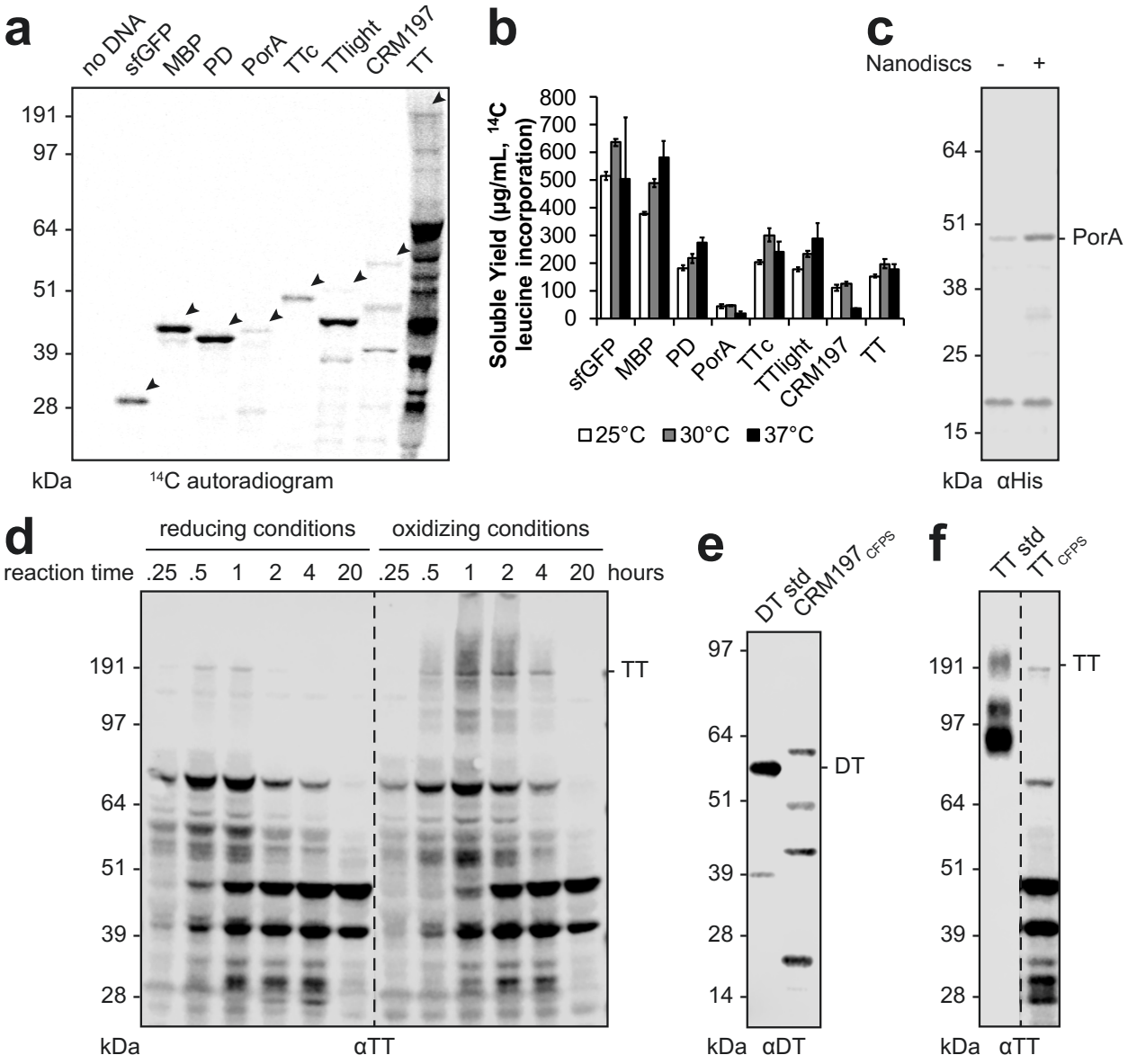

Figure S1. *In vitro* synthesis of licensed conjugate vaccine carrier proteins is possible over a range of temperatures and can be readily optimized. (**a**) ^{14}C autoradiogram analysis of soluble fractions from CFPS reactions shows no evidence of endogenous protein translation (no DNA control) and some fraction of full-length protein synthesis for all carriers tested. (**b**) With the exception of CRM197, all carriers expressed with similar soluble yields at 25°C, 30°C, and 37°C, as measured by ^{14}C-leucine incorporation. Values represent means and error bars represent standard deviations of biological replicates (n = 3). (**c**) Soluble expression of PorA was improved through the addition of lipid nanodiscs to the reaction. (**d**) Expression of full-length TT was enhanced by (i) performing *in vitro* protein synthesis in oxidizing conditions to improve assembly of the disulfide-bonded heavy and light chains into full-length TT and (ii) allowing reactions to run for only 2 h to minimize protease degradation. (**e**) CRM197 and (**f**) TT produced in CFPS reactions are detected with α-DT and α-TT antibodies, respectively, and are comparable in size to commercially available purified DT and TT protein standards (50 ng standard loaded). Images are representative of at least three biological replicates. Dashed line indicates samples are from the same blot with the same exposure. Molecular weight ladders are shown at the left of each image.

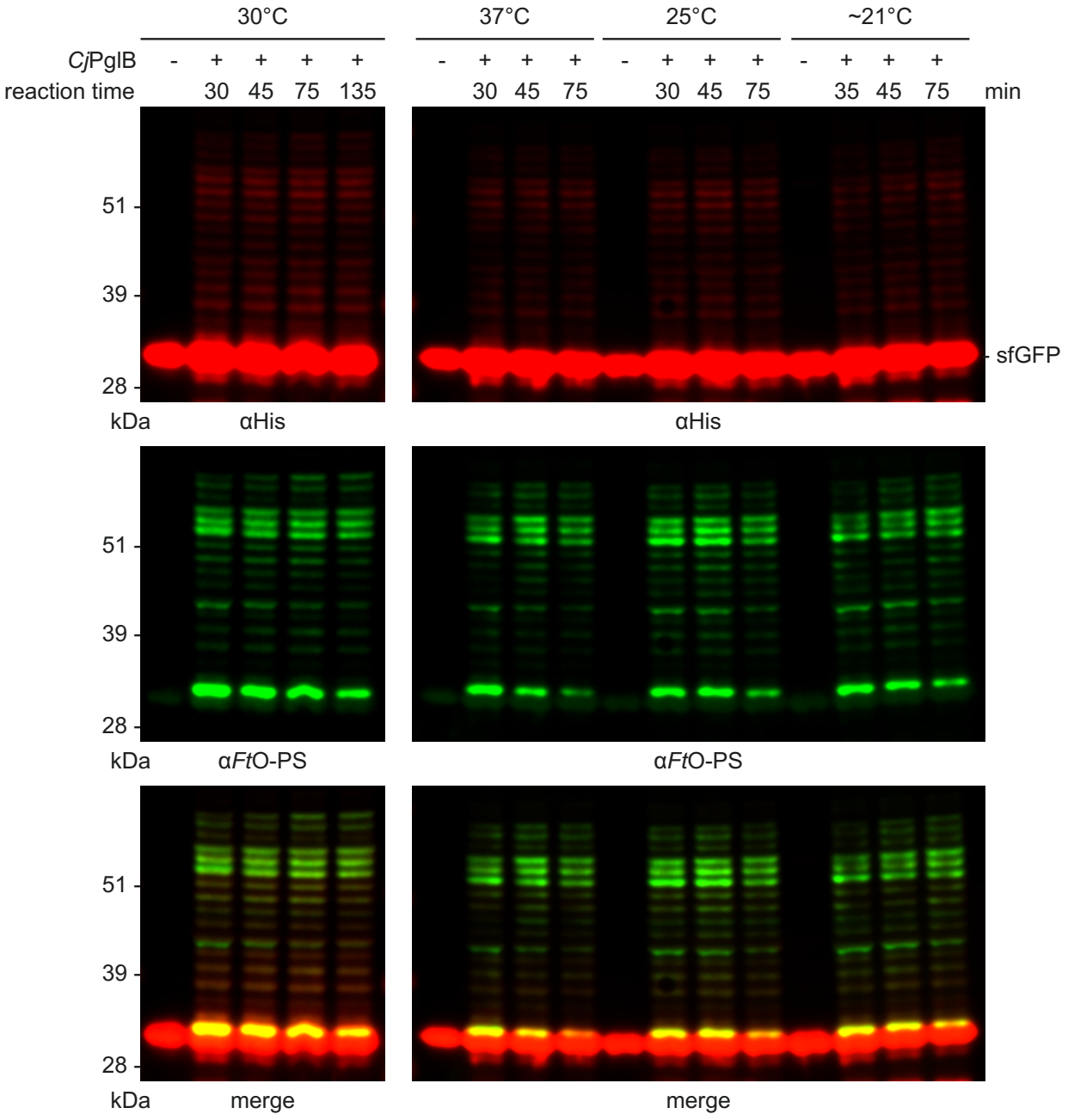

Figure S2. Glycosylation in iVAX reactions occurs in 1 h over a range of temperatures. Kinetics of *Ft*O-PS glycosylation at 30°C (**left**), 37°C, 25°C, and room temperature (~21°C) (**right**) are comparable and show that protein synthesis and glycosylation occur in the first hour of the iVAX reaction. These results demonstrate that the iVAX platform can synthesize conjugates over a range of permissible temperatures. Top panels show signal from probing with anti-hexa-histidine antibody (αHis) to detect the carrier protein, middle panels show signal from probing with commercial anti-*Ft*O-PS antibody (α*Ft*O-PS), and bottom panels show αHis and α*Ft*O-PS signals merged. Images are representative of at least three biological replicates. Molecular weight ladders are shown at the left of each image.

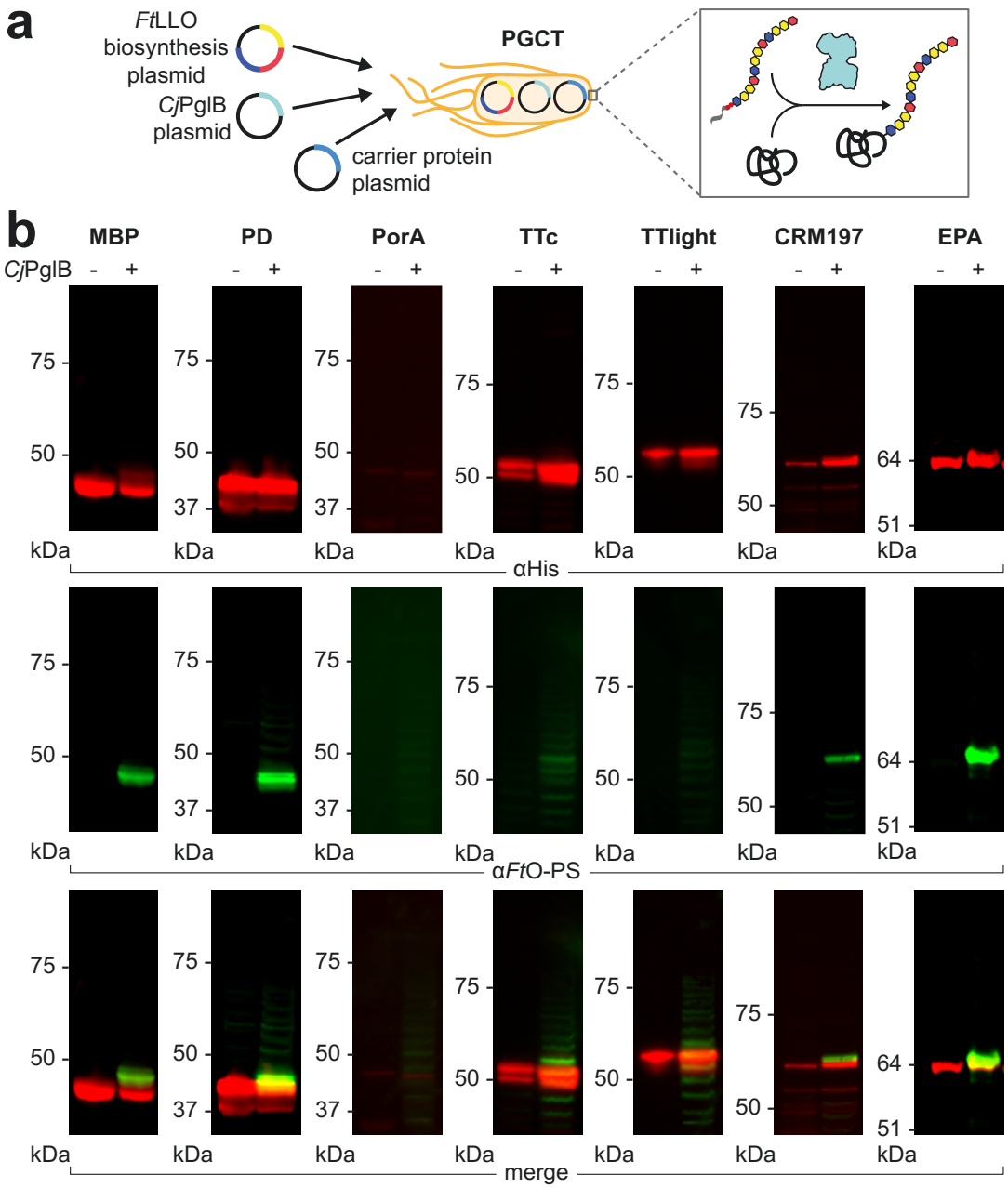

Figure S3. Production of conjugate vaccines against *F. tularensis* using PGCT in living *E. coli*. (**a**) Conjugates were produced via PGCT in CLM24 cells expressing *Cj*PglB, the biosynthetic pathway for *Ft*O-PS, and a panel of immunostimulatory carriers including those used in licensed vaccines. (**b**) We observed low expression of the licensed conjugate vaccine carrier proteins PorA and CRM197, compared to iVAX-derived samples. Top panels show signal from probing with anti-hexa-histidine antibody (αHis) to detect the carrier protein, middle panels show signal from probing with commercial anti-*Ft*O-PS antibody (α*Ft*O-PS), and bottom panels show αHis and α*Ft*O-PS signals merged. Images are representative of at least three biological replicates. Molecular weight ladders are shown at the left of each image.

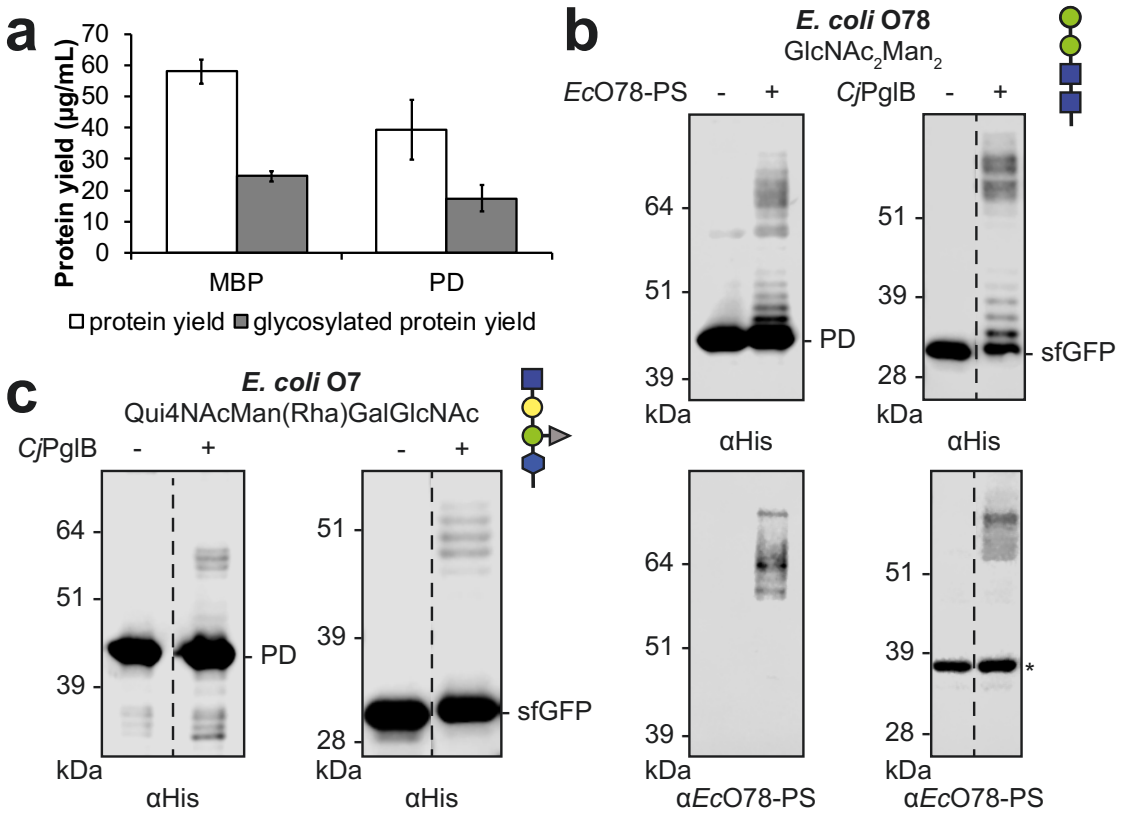

Figure S4. The iVAX platform is modular and can be used to synthesize clinically relevant yields of diverse conjugate vaccines. (**a**) Protein synthesis and glycosylation with *Ft*O-PS were measured in iVAX reactions producing MBP^{4xDQNAT} and PD^{4xDQNAT}. After ~1 h, reactions produced ~40 μg mL^{-1} protein, as measured via ^{14}C-leucine incorporation, of which ~20 μg mL^{-1} was glycosylated with *Ft*O-PS, as determined by densitometry. Values represent means and error bars represent standard errors of biological replicates (n = 2). To demonstrate modularity, iVAX lysates were prepared from cells expressing *Cj*PglB and biosynthetic pathways for either (**b**) the *E. coli* O78 antigen or (**c**) the *E. coli* O7 antigen and used to synthesize PD^{4xDQNAT} (**left**) or sfGFP$^{217\text{-}DQNAT}$ (**right**) conjugates. The structure and composition of the repeating monomer unit for each antigen is shown. Both polysaccharide antigens are compositionally and, in the case of the O7 antigen, structurally distinct compared to the *F. tularensis* O antigen. Blots show signal from probing with anti-hexa-histidine antibody (αHis) to detect the carrier protein. If a commercial anti-O-PS serum or antibody was available, it was used to confirm the identity of the conjugated O antigen (α-*Ec*O78 blots, panel **b**). Asterisk denotes bands resulting from non-specific serum antibody binding. Images are representative of at least three biological replicates. Dashed lines indicate samples are from nonadjacent lanes of the same blot with the same exposure. Molecular weight ladders are shown at the left of each image.

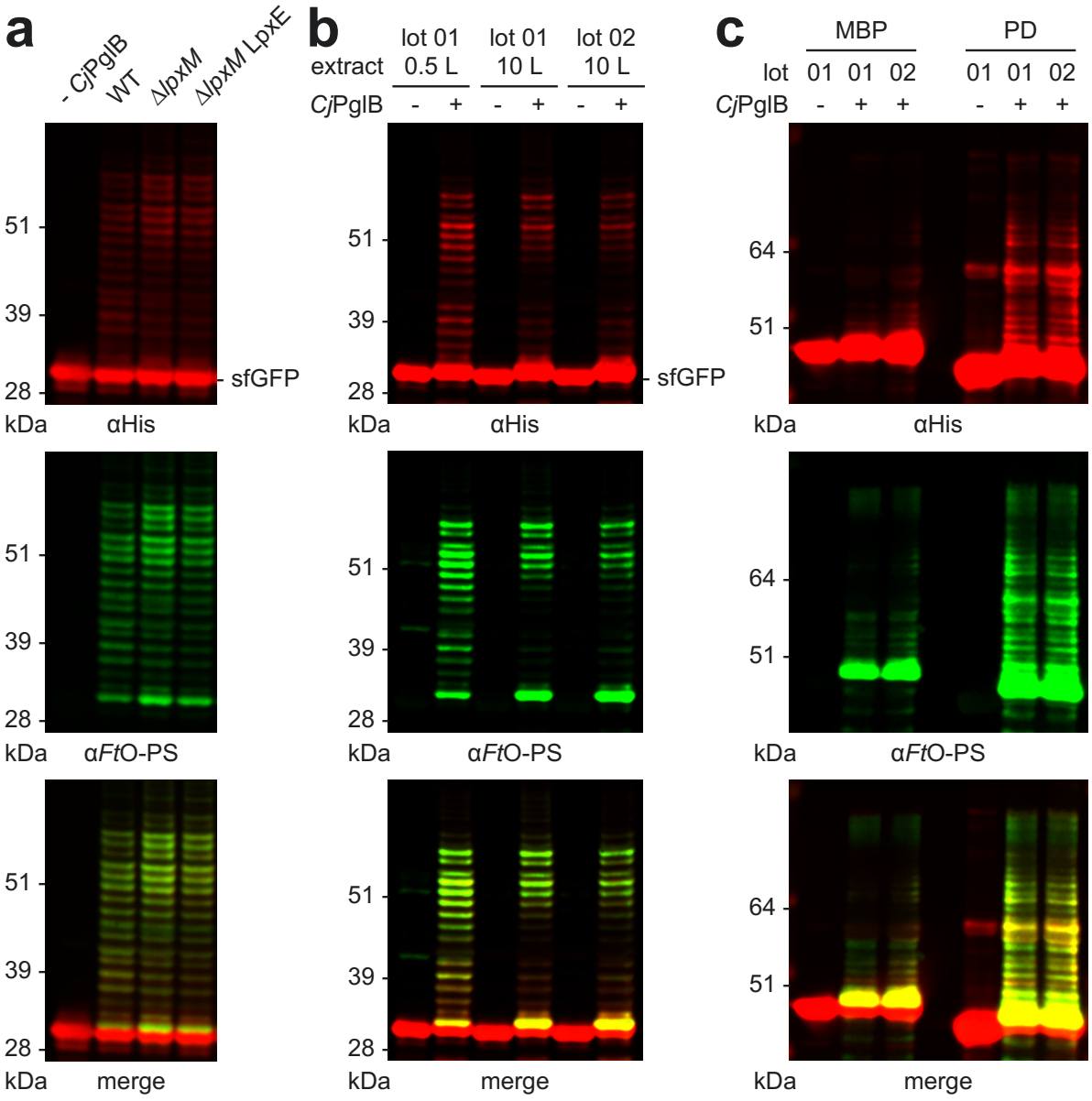

Figure S5. Detoxified lysate production and freeze-dried reactions scale reproducibly. (**a**) iVAX lysates containing *Cj*PglB and *Ft*O-PS were prepared from wild-type CLM24, CLM24 Δ*lpxM*, or CLM24 Δ*lpxM* cells expressing *Ft*LpxE. Lysates from engineered strains retained the ability to glycosylate sfGFP$^{217\text{-}DQNAT}$ with *Ft*O-PS. (**b**) Fermentations to produce endotoxin-edited iVAX lysates were scaled from 0.5 L to 10 L. We observed similar levels glycosylation at large and small scale and across different batches of lysate from 10 L fermentations (average glycosylation efficiencies of sfGFP$^{217\text{-}DQNAT}$ using lysates from 0.5 L and 10 L fermentations were 69 ± 5% and 69 ± 1% by densitometry, respectively). (**c**) For immunizations, we prepared two lots of *Ft*O-PS-conjugated MBP^{4xDQNAT} and PD^{4xDQNAT} from 5 mL freeze-dried iVAX reactions. We observed similar levels of purified protein (~200 µg) and *Ft*O-PS modification (66 ± 11% for MBP^{4xDQNAT} and 70 ± 1% for PD^{4xDQNAT} by densitometry) across both carriers and lots of material. Top panels show signal from probing with anti-hexa-histidine antibody (αHis) to detect the carrier protein, middle panels show signal from probing with commercial anti-*Ft*O-PS antibody (α*Ft*O-PS), and bottom panels show αHis and α*Ft*O-PS signals merged. Images are representative of at least three biological replicates. Molecular weight ladders are shown at left.

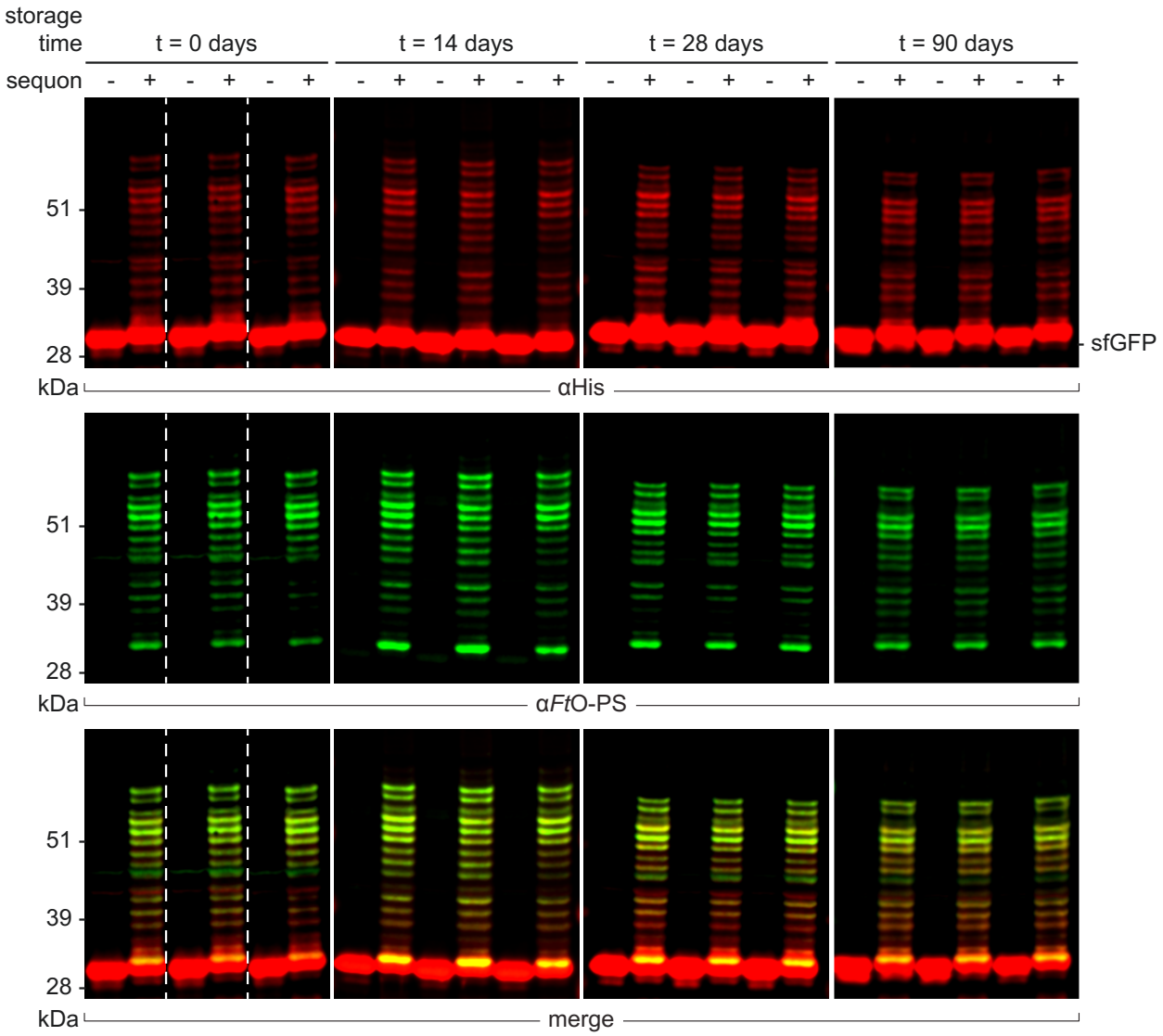

Figure S6. iVAX reactions are stable under ambient temperature storage conditions for at least 3 months. Stability of iVAX reactions was tested over a period of 3 months using economic packaging materials. Specifically, we vacuum sealed reactions using a commercial FoodSaver® appliance with Dri-Card™ desiccant cards enclosed to prevent rehydration of the iVAX pellets. At each time point, n = 3 reactions were rehydrated with plasmid encoding sfGFP$^{217\text{-}AQNAT}$ (- sequon) or sfGFP$^{217\text{-}DQNAT}$ (+ sequon). The average amount of protein synthesized across all replicates and time points was 19.78 ± 3.12 μg mL^{-1} (n = 12). These results show that iVAX reactions are stable at room temperature for at least 3 months, with no observable differences in protein synthesis or glycosylation activity, highlighting their potential for portable, on-demand conjugate vaccine production. Top panels show signal from probing with anti-hexa-histidine antibody (αHis) to detect the carrier protein, middle panels show signal from probing with commercial anti-*Ft*O-PS antibody (α*Ft*O-PS), and bottom panels show αHis and α*Ft*O-PS signals merged. Dashed lines indicate samples are from nonadjacent lanes of the same blot with the same exposure. Molecular weight ladders are shown at the left of each image.

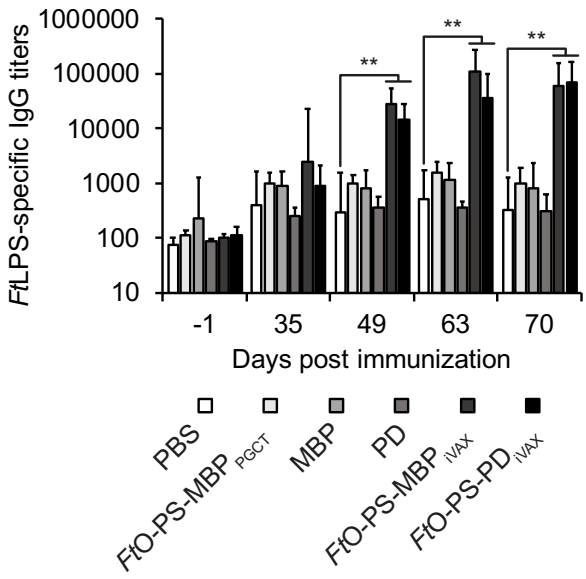

Figure S7. *Ft*LPS-specific antibody titers in vaccinated mice over time. Six groups of BALB/c mice were immunized subcutaneously with PBS or 7.5 µg of purified, cell-free synthesized unmodified $MBP^{4xDQNAT}$, *Ft*O-PS-conjugated $MBP^{4xDQNAT}$, unmodified $PD^{4xDQNAT}$, or *Ft*O-PS-conjugated $PD^{4xDQNAT}$. *Ft*O-PS-conjugated $MBP^{4xDQNAT}$ prepared in living *E. coli* cells using PCGT was used as a positive control. Each group was composed of six mice except for the PBS control group, which was composed of five mice. Mice were boosted on days 21 and 42 with identical doses of antigen. *Ft*LPS-specific IgG titers were measured by ELISA in serum collected on day -1, 35, 49, 63, and 70 following initial immunization. iVAX-derived conjugates elicited significantly higher levels of *Ft*LPS-specific IgG compared to compared to the PBS control group in serum collected on day 35, 49, and 70 of the study (**$p < 0.01$, Tukey-Kramer HSD). Values represent means and error bars represent standard errors of *Ft*LPS-specific IgGs detected by ELISA.

Table S1. Cost analysis for iVAX reactions. The total cost to assemble iVAX reactions is calculated below. A 1 mL iVAX reaction produces two 10 μg vaccine doses and can be assembled for $11.75. In the table, amino acid cost accounts for 2 mM each of the 20 canonical amino acids purchased individually from Sigma. Lysate cost is based on a single employee making 50 mL lysate from a 10 L fermentation, assuming 30 lysate batches per year and a 5-year equipment lifetime. Component source is also included in the table if it is available to purchase directly from a supplier. Homemade components cannot be purchased directly and must be prepared according to procedures described in the Materials and Methods section.

Component	Cost ($/mL rxn)	Supplier	Product No
$Mg(Glu)_2$	<0.00	Sigma	49605
NH_4Glu	<0.00	MP	02180595
KGlu	<0.00	Sigma	G1501
ATP	0.01	Sigma	A2383
GTP	0.27	Sigma	G8877
UTP	0.23	Sigma	U6625
CTP	0.20	Sigma	C1506
Folinic acid	0.02	Sigma	47612
tRNA	0.21	Roche	10109541001
Amino acids	<0.00	homemade	
PEP	1.79	Roche	10108294001
NAD	0.07	Sigma	N8535-15VL
CoA	0.34	Sigma	C3144
Oxalic acid	<0.00	Sigma	P0963
Putrescine	<0.00	Sigma	P5780
Spermidine	<0.00	Sigma	S2626
HEPES	<0.00	Sigma	H3375
$MnCl_2$	<0.00	Sigma	63535
DDM	0.36	Anatrace	D310S
Plasmid	0.88	homemade	
Lysate	7.37	homemade	
Total	**11.75**	**$/mL rxn**	
	5.88	**$/dose**	

Table S2. Plasmids used in this study.

Plasmid	Description	Source
pSF-*Cj*PglB	*C. jejuni* PglB with a C-terminal 1xFLAG epitope tag in pSF, a modified pBAD expression vector	(*13*)
pGAB2	*F. tularensis* O-PS antigen gene cluster in pLAFR1	(*6*)
pMW07-O78	*E. coli* O78 antigen gene cluster in pMW07	(*14*)
pJHCV32	*E. coli* O7 antigen gene cluster in pVK102	(*15*)
pKD46	Encodes λ red system for recombineering	(*4*)
pKD4	Encodes kanamycin resistance cassette with upstream and downstream FRT sites	(*4*)
pCP20	Encodes *flp* for Flp-FRT recombination	(*4*)
pSF-*Cj*PglB-LpxE	*C. jejuni* PglB with a C-terminal 1xFLAG epitope tag and *F. tularensis* LpxE in pSF	This work; Addgene 128389
pJL1-sfGFP$^{217\text{-}DQNAT}$	Superfolder green fluorescent protein variant modified after residue T216 with 21 amino acid insertion containing the *C. jejuni* AcrA N123 glycosylation site but with an optimal DQNAT glycosylation sequence and a C-terminal 6xHis tag	(*16*)
pJL1-sfGFP$^{217\text{-}AQNAT}$	Same as pJL1 sfGFP$^{217\text{-}DQNAT}$, but with an AQNAT glycosylation sequence that is not modified by *Cj*PglB	(*16*)
pJL1-MBP^{4xDQNAT}	*E. coli* maltose binding protein with a C-terminal 4xDQNAT glycosylation tag and a 6xHis tag in pJL1, a T7-driven *in vitro* expression vector	This work; Addgene 128390
pJL1-PD^{4xDQNAT}	*H. influenzae* protein D with a C-terminal 4xDQNAT glycosylation tag and a 6xHis tag in pJL1	This work; Addgene 128391
pJL1-PorA^{4xDQNAT}	*N. meningitidis* PorA porin protein with a C-terminal 4xDQNAT glycosylation tag and a 6xHis tag in pJL1	This work; Addgene 128392
pJL1-TTc^{4xDQNAT}	Fragment C domain of *C. tetani* toxin with a C-terminal 4xDQNAT glycosylation tag and a 6xHis tag in pJL1	This work; Addgene 128393
pJL1-TTlight^{4xDQNAT}	Light chain variant of *C. tetani* toxin containing an inactivating E234A mutation in the enzyme active site with a C-terminal 4xDQNAT glycosylation tag and a 6xHis tag in pJL1	This work; Addgene 128394
pJL1-CRM197^{4xDQNAT}	*C. diphtheriae* toxin variant with an inactivating G52E mutation in the enzyme active site with a C-terminal 4xDQNAT glycosylation tag and a 6xHis tag in pJL1	This work; Addgene 128395
pJL1-TT^{4xDQNAT}	*C. tetani* toxin variant containing an inactivating E234A mutation in the enzyme active site with a C-terminal 4xDQNAT glycosylation tag and a 6xHis tag in pJL1	This work; Addgene 128396
pJL1-EPA$^{DNNNS\text{-}DQNRT}$	*P. aeruginosa* exotoxin A containing a DNNNS glycosylation site at residue 242 and a DQNRT glycosylation site at residue 384 and a C-terminal 6xHis tag in pJL1	This work; Addgene 128397

Table S2 (continued). Plasmids used in this study.

Plasmid	Description	Source
pTrc99s-ssDsbA-MBP^{4xDQNAT}	*E. coli* maltose binding protein with an N-terminal DsbA signal sequence for periplasmic translocation and a C-terminal 4xDQNAT glycosylation tag and a 6xHis tag in pTrc99s	This work; Addgene 128398
pTrc99s-ssDsbA-PD^{4xDQNAT}	*H. influenzae* protein D with an N-terminal DsbA signal sequence for periplasmic translocation and a C-terminal 4xDQNAT glycosylation tag and a 6xHis tag in Trc99s	This work; Addgene 128399
pTrc99s-ssDsbA-PorA^{4xDQNAT}	*N. meningitidis* PorA porin protein with an N-terminal DsbA signal sequence for periplasmic translocation and a C-terminal 4xDQNAT glycosylation tag and a 6xHis tag in pTrc99s	This work; Addgene 128400
pTrc99s-ssDsbA-TTc^{4xDQNAT}	Fragment C domain of *C. tetani* toxin with an N-terminal DsbA signal sequence for periplasmic translocation and a C-terminal 4xDQNAT glycosylation tag and a 6xHis tag in pTrc99s	This work; Addgene 128401
pTrc99s-ssDsbA-TTlight^{4xDQNAT}	Light chain variant of *C. tetani* toxin containing an inactivating E234A mutation in the enzyme active site with an N-terminal DsbA signal sequence for periplasmic translocation and a C-terminal 4xDQNAT glycosylation tag and a 6xHis tag in pTrc99s	This work; Addgene 128402
pTrc99s-ssDsbA-CRM197^{4xDQNAT}	*C. diphtheriae* toxin variant with an inactivating G52E mutation in the enzyme active site with an N-terminal DsbA signal sequence for periplasmic translocation and a C-terminal 4xDQNAT glycosylation tag and a 6xHis tag in pTrc99s	This work; Addgene 128403
pTrc99s-ssDsbA-EPA$^{DNNNS-DQNRT}$	*P. aeruginosa* exotoxin A containing a DNNNS glycosylation site at residue 242 and a DQNRT glycosylation site at residue 384 with an N-terminal DsbA signal sequence for periplasmic translocation and a C-terminal 6xHis tag in pTrc99s	This work; Addgene 128404

Table S3. Primers used to generate CLM24 Δ*lpxM*. Primers used to construct and verify the CLM24 Δ*lpxM* strain are listed below. KO primers were used for amplification of the kanamycin resistance cassette from pKD4 with homology to *lpxM*. Seq primers were used for colony PCRs and sequencing confirmation of knockout strains.

Primer Name	DNA Sequence (5' to 3')
lpxM KO for	TACACTATCACCAGATTGATTTTTGCCTTATCCGAAACTGGAAAAGCATGGTGTAGGCTGGAGCTGCTTC
lpxM KO rev	GCGAAGGCCTCTCCTCGCGAGAGGCTTTTTTATTTGATGGGATAAAGATCCATATGAATATCCTCCTTAGTTCCTATTC
lpxM seq for	AGTACCGGCTTTTTTTATTTGG
lpxM seq rev	CTAATACCACGCGTATTTTAACG

Table S4. Antibodies and antisera used in this study.

Target	Source	Dilution
Rabbit pAb to 6xHis epitope tag	Abcam	1:7500
Mouse mAb FB11 to *F. tularensis* LPS	Abcam	1:5000
Rabbit pAb to *E. coli* O78 antigen	Abcam	1:2500
Rabbit pAb to *C. diphtheriae* toxin	Abcam	1:2000
Rabbit pAb to *C. tetani* toxin	Abcam	1:2000
Goat anti-rabbit IgG IR dye 680	LI-COR	1:15000-1:10000
Goat anti-rabbit IgG IR dye 800	LI-COR	1:15000-1:10000
Goat anti-mouse IgG IR dye 800	LI-COR	1:15000-1:10000
Goat anti-mouse IgG HRP	Abcam	1:25,000
Goat anti-mouse IgG1 HRP	Abcam	1:25,000
Goat anti-mouse IgG2a HRP	Abcam	1:25,000

References and Notes

1. M. F. Feldman *et al.*, Engineering N-linked protein glycosylation with diverse O antigen lipopolysaccharide structures in Escherichia coli. *Proc Natl Acad Sci U S A* **102**, 3016-3021 (2005).

2. A. C. Fisher *et al.*, Production of secretory and extracellular N-linked glycoproteins in Escherichia coli. *Appl Environ Microbiol* **77**, 871-881 (2011).

3. B. D. Needham *et al.*, Modulating the innate immune response by combinatorial engineering of endotoxin. *Proc Natl Acad Sci U S A* **110**, 1464-1469 (2013).

4. K. A. Datsenko, B. L. Wanner, One-step inactivation of chromosomal genes in Escherichia coli K-12 using PCR products. *Proc Natl Acad Sci U S A* **97**, 6640-6645 (2000).

5. A. A. Ollis *et al.*, Substitute sweeteners: Diverse bacterial oligosaccharyltransferases with unique N-glycosylation site preferences. *Sci Rep* **5**, 15237 (2015).

6. J. Cuccui *et al.*, Exploitation of bacterial N-linked glycosylation to develop a novel recombinant glycoconjugate vaccine against Francisella tularensis. *Open Biol* **3**, 130002 (2013).

7. M. C. Jewett, J. R. Swartz, Mimicking the Escherichia coli cytoplasmic environment activates long-lived and efficient cell-free protein synthesis. *Biotechnol Bioeng* **86**, 19-26 (2004).

8. J. A. Schoborg *et al.*, A cell-free platform for rapid synthesis and testing of active oligosaccharyltransferases. *Biotechnol Bioeng*, (2017).

9. D. M. Kim, J. R. Swartz, Efficient production of a bioactive, multiple disulfide-bonded protein using modified extracts of Escherichia coli. *Biotechnol Bioeng* **85**, 122-129 (2004).

10. D. J. Chen *et al.*, Delivery of foreign antigens by engineered outer membrane vesicle vaccines. *Proc Natl Acad Sci U S A* **107**, 3099-3104 (2010).

11. S. H. Hong *et al.*, Cell-free protein synthesis from a release factor 1 deficient Escherichia coli activates efficient and multiple site-specific nonstandard amino acid incorporation. *ACS Synth Biol* **3**, 398-409 (2014).

12. D. M. Kim, J. R. Swartz, Regeneration of adenosine triphosphate from glycolytic intermediates for cell-free protein synthesis. *Biotechnol Bioeng* **74**, 309-316 (2001).

13. A. A. Ollis, S. Zhang, A. C. Fisher, M. P. DeLisa, Engineered oligosaccharyltransferases with greatly relaxed acceptor-site specificity. *Nat Chem Biol* **10**, 816-822 (2014).

14. E. Celik *et al.*, Glycoarrays with engineered phages displaying structurally diverse oligosaccharides enable high-throughput detection of glycan-protein interactions. *Biotechnol J* **10**, 199-209 (2015).

15. M. A. Valvano, J. H. Crosa, Molecular cloning and expression in Escherichia coli K-12 of chromosomal genes determining the O7 lipopolysaccharide antigen of a human invasive strain of E. coli O7:K1. *Infect Immun* **57**, 937-943 (1989).

16. T. Jaroentomeechai *et al.*, Single-pot glycoprotein biosynthesis using a cell-free transcription-translation system enriched with glycosylation machinery. *Nat Commun* **9**, 2686 (2018).